J Physiol 594.12 (2016) pp 3317–3338

The Journal of Physiology

Spontaneous Ca^{2+} transients in interstitial cells of Cajal located within the deep muscular plexus of the murine small intestine

Salah A. Baker[1,*], Bernard T. Drumm[1,*], Dieter Saur[2], Grant W. Hennig[1], Sean M. Ward[1] and Kenton M. Sanders[1]

[1] *Department of Physiology and Cell Biology, University of Nevada School of Medicine, Reno, NV, USA*
[2] *II. Medizinische Klinik und Poliklinik, Klinikum rechts der Isar der TU München, München, Germany*

Key points

- Interstitial cells of Cajal at the level of the deep muscular plexus (ICC-DMP) in the small intestine generate spontaneous Ca^{2+} transients that consist of localized Ca^{2+} events and limited propagating Ca^{2+} waves.
- Ca^{2+} transients in ICC-DMP display variable characteristics: from discrete, highly localized Ca^{2+} transients to regionalized Ca^{2+} waves with variable rates of occurrence, amplitude, duration and spatial spread.
- Ca^{2+} transients fired stochastically, with no cellular or multicellular rhythmic activity being observed. No correlation was found between the firing sites in adjacent cells.
- Ca^{2+} transients in ICC-DMP are suppressed by the ongoing release of inhibitory neurotransmitter(s).
- Functional intracellular Ca^{2+} stores are essential for spontaneous Ca^{2+} transients, and the sarco/endoplasmic reticulum Ca^{2+}-ATPase (SERCA) pump is necessary for maintenance of spontaneity.
- Ca^{2+} release mechanisms involve both ryanodine receptors (RyRs) and inositol triphosphate receptors ($InsP_3Rs$). Release from these channels is interdependent.
- ICC express transcripts of multiple RyRs and $InsP_3Rs$, with *Itpr1* and *Ryr2* subtypes displaying the highest expression.

Abstract Interstitial cells of Cajal in the deep muscular plexus of the small intestine (ICC-DMP) are closely associated with varicosities of enteric motor neurons and generate responses contributing to neural regulation of intestinal motility. Responses of ICC-DMP are mediated by activation of Ca^{2+}-activated Cl^- channels; thus, Ca^{2+} signalling is central to the behaviours of these cells. Confocal imaging was used to characterize the nature and mechanisms of Ca^{2+} transients in ICC-DMP within intact jejunal muscles expressing a genetically encoded Ca^{2+} indicator (GCaMP3) selectively in ICC. ICC-DMP displayed spontaneous Ca^{2+} transients that ranged from discrete, localized events to waves that propagated over variable distances. The occurrence of Ca^{2+} transients was highly variable, and it was determined that firing was stochastic in nature. Ca^{2+} transients were tabulated in multiple cells within fields of view, and no correlation was found between the events in adjacent cells. TTX (1 μM) significantly increased the occurrence of Ca^{2+} transients, suggesting that ICC-DMP contributes to the tonic inhibition conveyed by ongoing activity of inhibitory motor neurons. Ca^{2+} transients were minimally affected after 12 min in Ca^{2+} free solution, indicating these events do not depend immediately upon Ca^{2+} influx. However,

*These authors contributed equally to this work.

DOI: 10.1113/JP271699

inhibitors of sarco/endoplasmic reticulum Ca^{2+}-ATPase (SERCA) pump and blockers of inositol triphosphate receptor ($InsP_3R$) and ryanodine receptor (RyR) channels blocked ICC Ca^{2+} transients. These data suggest an interdependence between RyR and $InsP_3R$ in the generation of Ca^{2+} transients. *Itpr1* and *Ryr2* were the dominant transcripts expressed by ICC. These findings provide the first high-resolution recording of the subcellular Ca^{2+} dynamics that control the behaviour of ICC-DMP *in situ*.

(Received 6 October 2015; accepted after revision 24 January 2016; first published online 29 January 2016)
Corresponding author K. M. Sanders: Department of Physiology and Cell Biology, University of Nevada School of Medicine, MS 352, Reno, NV 89557, USA. Email: ksanders@medicine.nevada.edu

Abbreviations 2-APB, 2-aminoethyl diphenylborinate; CaCC, Ca^{2+}-activated Cl^- channel; CPA, cyclopiazonic acid; EFS, electrical field stimulation; eGFP, enhanced green fluorescent protein; FACS, fluorescence-activated cell sorting; FOV, field of view; GI, gastrointestinal; ICC, interstitial cells of Cajal; ICC-DMP, interstitial cells of Cajal at the level of the deep muscular plexus; ICC-IM, intramuscular interstitial cells of Cajal; ICC-MY, myenteric interstitial cells of Cajal; GCaMP3, genetically encoded Ca^{2+} indicator composed of a single GFP; $InsP_3R$, inositol triphosphate receptor; KRB, Krebs-Ringer bicarbonate; PBS, phosphate-buffered saline; PDGFR, platelet derived growth factor receptor; qPCR, quantitative PCR; ROI, regions of interest; RyR, ryanodine receptor; SERCA, sarco/endoplasmic reticulum Ca^{2+}-ATPase; SIP, smooth muscle, interstitial cells of Cajal, platelet derived growth factor receptor α; SIP syncytium, electrical syncytium formed by smooth muscle cells, interstitial cells of Cajal and platelet derived growth factor receptor α^+ cells in GI muscles; SMC, smooth muscle cells; SNR, signal-to-noise ratio; ST, spatio-temporal; STIC, spontaneous transient inward current; XeC, xestospongin C.

Introduction

Interstitial cells of Cajal (ICC) generate the pacemaker activity that drives electrical (slow waves) and contractile rhythmicity in organs of the gastrointestinal (GI) tract (Langton *et al.* 1989; Ward *et al.* 1994; Huizinga *et al.* 1995; Dickens *et al.* 1999; Ordog *et al.* 1999; Sanders *et al.* 2014*b*). However, specialized populations of ICC distributed in the deep muscular plexus of the small intestine (ICC-DMP) and in muscle bundles (intramuscular ICC; ICC-IM) in other smooth muscles of the GI tract appear to lack the ability to generate slow waves. ICC-DMP and ICC-IM are closely apposed to enteric nerve terminals and transduce part of the postjunctional responses to neurotransmitters released from enteric motor neurons (Daniel & Posey-Daniel, 1984; Burns *et al.* 1996; Ward *et al.* 2000; Beckett *et al.* 2005; Blair *et al.* 2012; Klein *et al.* 2013; Sanders *et al.* 2014*a*).

Ca^{2+} handling mechanisms appear to be important for the behaviours of all classes of ICC in the GI tract because these cells have prominent expression of ANO1, a type of Ca^{2+}-activated Cl^- channel (CaCC) (Gomez-Pinilla *et al.* 2009; Zhu *et al.* 2009). CaCC are responsible for the generation of spontaneous transient inward currents (STICs) in ICC (Zhu *et al.* 2011), and these events probably cause the spontaneous transient depolarizations (or 'unitary potentials') recorded from intact muscles (Edwards *et al.* 1999; van Helden *et al.* 2000; Suzuki *et al.* 2003). Generation of STICs depends upon localized Ca^{2+} signalling in cells (ZhuGe *et al.* 1998), although the sources, regulation, co-ordination between cellular release sites and spatial spread of Ca^{2+} transients in ICC are poorly understood. Previous studies of Ca^{2+} events in ICC have depended upon loading of Ca^{2+} indicators and have concentrated on the monitoring of global Ca^{2+} events (Park *et al.* 2006; Lee *et al.* 2009; Lowie *et al.* 2011; Huizinga *et al.* 2014; Wang *et al.* 2014). The inherent limitations of Ca^{2+} indicators, loading procedures that fill several types of cells within fields of view (FOVs) and significant photobleaching have allowed very limited spatial and temporal resolution, sometimes including poor signal-to-noise levels, contamination of signals from other cell types and poor resolution of subcellular events. Furthermore, the single study that has described the activity of an intramuscular type of ICC (i.e. ICC-DMP) (Huizinga *et al.* 2014) was limited by the factors described above.

In the present study, we utilized the inducible Cre/loxP technique to express a genetically-encoded Ca^{2+} biosensor (GCaMP3) in a cell-specific manner in ICC-DMP. We investigated the sites of origin of spontaneous Ca^{2+} transients, spatial spread of spontaneous Ca^{2+} transients and the source(s) of Ca^{2+} transients in an intramuscular type of ICC, a class of ICC that previously has received little attention. We hypothesized that subcellular Ca^{2+} events must be relatively localized and transient in ICC-DMP to explain the STICs that appear to be the dominant pattern of electrophysiological behaviour in intramuscular ICC (Zhu *et al.* 2009). We also hypothesized that Ca^{2+} transients in ICC-DMP must be discrete cellular events with little or no cell-to-cell propagation because ICC-DMP fail to develop slow wave-like depolarizations, as seen in the myenteric interstitial cells of Cajal (ICC-MY) of the small intestine. ICC-DMP were considered ideal for this initial study of intramuscular ICC because they are concentrated within a small volume of tissue

and are probably innervated and regulated by motor neurons (Ward *et al.* 2000; Ward & Sanders, 2001; Wang *et al.* 2003; Iino *et al.* 2004). Cell-specific expression of GCaMP3 allowed imaging of subcellular Ca^{2+} transients *in situ* with very high signal-to-noise ratios and with excellent spatio-temporal (ST) resolution. The intact tissue preparations allowed several ICC-DMP to be imaged within the same Z-plane simultaneously, and so information about intercellular communication and entrainment of Ca^{2+} signalling in adjacent cells could be investigated during relatively long periods of imaging.

Methods

Animals

B6.129S-*Gt(ROSA)26Sor*$^{tm38(CAG\text{-}GCaMP3)Hze}$/J (GCaMP3 mice) and their wild-type siblings (C57BL/6) were obtained from the Jackson Laboratory (Bar Harbor, MN, USA). B6.129S7-*Kit*^{tm1Rosay}/J (Kit$^{+/copGFP}$ mice) were generated and bred in house (Ro *et al.* 2010). c-Kit$^{+/Cre\text{-}ERT2}$ (Kit-Cre mice) were developed by Dr Dieter Saur (Technical University Munich, Munich, Germany).

Mice between 6 and 8 weeks of age were treated with tamoxifen (see below) and used for experiments after 10 days. On the days of experimentation, the animals were anaesthetized by inhalation of isoflurane (Baxter, Deerfield, IL, USA) and killed by cervical dislocation.

The Institutional Animal Use and Care Committee at the University of Nevada, Reno, approved all of the procedures. The animals used and the experiments performed in the present study were in accordance with the National Institutes of Health Guide for the Care and Use of Laboratory Animals.

Tamoxifen preparation and administration

We cross-bred GCaMP3 mice with Kit-Cre mice (described above) and refer to the offspring as Kit-Cre-GCaMP3 mice. The mice were injected with tamoxifen to induce Cre and subsequent GCaMP3 expression.

Tamoxifen (80 mg; T5648; Sigma-Aldrich, St Louis, MO, USA) was dissolved in 800 μl of ethanol (200 proof, absolute, anhydrous; Pharmco-Aaper, Shelbyville, KY, USA) by vortexing for 20 min. Next, 3.2 ml of safflower (generic) was added to make solutions of 20 mg ml^{-1} and then sonicated for 30 min prior to injection.

Each animal was injected (I.P.) with 0.1 ml of tamoxifen solution (2 mg of tamoxifen) for three consecutive days. Mice were used 10 days after the initial injection and the expression of GCaMP3 was also confirmed by genotyping.

Tissue preparation

After an abdominal incision, small segments of the jejunum (length 2 cm) were removed from mice and were bathed in Krebs-Ringer bicarbonate solution (KRB). The segments were opened along the mesenteric border and intraluminal contents were washed away with KRB. The mucosa layers were removed by sharp dissection.

Drugs and solutions

Tissues were maintained and perfused with KRB containing (mmol l^{-1}): 120.35 NaCl, 5.9 KCl, 15.5 $NaHCO_3$, 1.2 NaH_2PO_4, 1.2 $MgCl_2$, 2.5 $CaCl_2$ and 11.5 glucose. KRB was bubbled with a mixture of 97 % O_2 –3 % CO_2 and warmed to a physiological temperature of 37 $\pm$ 0.2°C. For experiments with 0 mM $[Ca^{2+}]_o$, no $CaCl_2$ was added to the KRB; thus, the solutions were nominally free of Ca^{2+}, although there may have been trace amounts of Ca^{2+} in these solutions. We refer to this as a 0 mM external Ca^{2+} solution.

2-aminoethyl diphenylborinate (2-APB), cyclopiazonic acid (CPA), ryanodine, thapsigargin and xestospongin C (XeC) were purchased from Sigma-Aldrich. TTX was purchased from Tocris Bioscience (Ellisville, MO, USA). All drugs were dissolved in the solvent recommended by the manufacturer and the final concentration is stated as appropriate.

Immunohistochemistry

Whole mount sections of jejunum were studied using single- or double-labelling immunohistochemistry. Tissues were fixed in paraformaldehyde (4% w/v; 4°C; 10 min) as described previously (Baker *et al.* 2015). Following fixation, tissues were washed in phosphate-buffered saline (PBS; 0.1 M; overnight) and incubated in BSA (1%; room temperature for 1 h). Tissues were subsequently incubated with primary and secondary antibodies. The antibodies used were goat polyclonal antibody raised against c-Kit (mSCFR, dilution 1:500 in PBS; R&D Systems, Minneapolis, MN, USA) and chicken polyclonal antibody raised against GFP (dilution 1:1000; Abcam Inc. Cambridge, MA, USA). Control experiments were performed using single immunolabelling of tissues and omitting either primary or secondary antibodies. Control experiments were also performed on: (i) intestinal muscles from Kit-Cre-GCaMP3 mice not injected with tamoxifen; (ii) Kit-Cre-GCaMP3 mice injected only with Safflower oil (vehicle control); and (iii) Kit-Cre mice injected with tamoxifen.

Immunoreactivity was detected using AlexaFluor-594 labelled donkey anti-goat IgG and AlexaFluor-488 labelled donkey anti-chicken IgG, respectively (dilution 1:1000 in PBS; Molecular Probes/Life Sciences, Carlsbad, CA USA). Whole mounts were examined with an LSM 510 Meta laser scanning confocal microscope (Zeiss, Thornwood, NY, USA) using a 40× 1.3 NA objective (Zeiss). Confocal micrographs displayed are digital composites of Z-series scans of 0.5–1.0 μm optical sections through a depth of

Table 1. Summary table of $InsP_3$ and RyR primer sequences

Gene	Primer sequences	GenBank accession number
mGapdh-F	CTGCACCACCAACTGCTTAG	NM_008084
mGapdh-R	AGTGGATGCAGGGATGATGT	
mItpr1-F	TTATCAGCACCTTAGGCTTGGTTGA	NM_010585
mItpr1-R	ATCTGTAGTGCTGTTGGCCCCG	
mItpr2-F	CAACCCAGGCTGCAAAGAGGTGA	NM_019923
mItpr2-R	AGGTCGTCCGAAGGAAAATGTGCT	
mItpr3-F	CTTTGGGGCTGGTGGATGACCGTTG	NM_080553
mItpr3-R	TGCAGCTTCTGCAGCAATACCACA	
mRyr1-F	GTCAGTTCGAGCCCTGCAGGAG	NM_009109
mRyr1-R	GCAACTCAGGTACATACGACTGTGT	
mRyr2-F	TCCCCCGGACCTGTCTATCTGC	NM_023868
mRyr2-R	GGCCTCCACCTTGAGCAGTCTTC	
mRyr3-F	TCCTCGTCAGTGTGTCCTCTGAAA	NM_177652
mRyr3-R	CATGGCCACCGAGTAAGTATCCTTC	

Genes for $InsP_3$ and RyR used in the present study are listed, including their name, primer sequences and GenBank accession numbers.

1–5 μm. Final images were constructed and montages were assembled using Zeiss LSM 5 Image Examiner and converted to Tiff files for final processing in Photoshop CS5 (Adobe Systems Inc., Mountain View, CA, USA) and Corel Draw, version 7.0 (Corel Corp., Ontario, Canada).

Intracellular microelectrode recordings

Intracellular microelectrode recordings were performed as described previously (Ward *et al.* 1994). Briefly, impalements of circular muscle cells were made with glass microelectrodes with resistances of 80–120 MΩ. Transmembrane potentials were recorded with a high impedance electrometer (Axon Instruments, Union City, CA, USA). Data were recorded on a PC running AxoScope, version 10 (Axon Instruments) and hard copies were made using Clampfit (Axon Instruments). Experiments were performed in the presence of nifedipine (1 μM) to reduce contractions and to facilitate impalements of cells for extended periods. Neural responses were elicited by square wave pulses of electrical field stimulation (EFS; 10 Hz, 0.5 ms pulse duration; 10–15 V; 1 s trains) delivered via two parallel platinum electrodes placed on either side of the muscle strips using a Grass stimulator as described above. EFS induced neural responses were abolished by pretreatment with TTX (1 μM, data not shown).

Cell isolation and fluorescence-activated cell sorting (FACS)

Jejunal ICC from $Kit^{+/copGFP}$ mice were dispersed from dissected segments (see above) by incubating them in Ca^{2+}-free Hank's solution for 30 min and then dispersing them as described previously (Baker *et al.* 2013). Kit positive (enhanced green fluorescent protein; eGFP) cells were sorted by FACS with a FACSAria II instrument (Becton-Dickinson Biosciences, Franklin Lakes, NJ, USA) using an excitation laser (488 nm) and emission filter (530/30 nm). Sorting was performed using a 130 μm nozzle at a sheath pressure of 12 psi and sort rate of 1,000 to 3,000 events s^{-1}. Live cells, gated on exclusion of Hoechst 33258 viability indicator (data not shown), were subsequently gated on eGFP fluorescence intensity.

RNA extraction and quantitative PCR

Total RNA was isolated from purified-sorted ICC and total jejunal cells before sorting (representing the total cell population from the tunica muscularis), using an illustra RNAspin Mini RNA Isolation Kit (GE Healthcare Ltd, Little Chalfont, UK) and first-strand cDNA was synthesized using SuperScript III (Invitrogen, Carlsbad, CA) in accordance with the manufacturer's instructions. The PCR primers used and their GenBank accession numbers are listed in Table 1. Using GoTaq DNA Polymerase (Promega, Madison, WI, USA), PCR products were analysed on 2% agarose gels and visualized by ethidium bromide. Quantitative PCR (qPCR) was performed with the same primers as PCR using SYBR green chemistry on the 7500 HT Real-time PCR System (Applied Biosystems, Foster City, CA, USA) and analysed as described previously (Baker *et al.* 2013). The data are plotted along with standard error bars and are derived from experiments on four tissues of four animals.

Calcium imaging

Jejunal muscle segments were pinned to the base of a Sylgard-coated dish. The preparation was perfused with warmed KRB solution at 37°C. After an equilibration period of 1 h, preparations were visualized and imaged using a spinning-disk confocal microscope (CSU-X1 spinning disk; Yokogawa Electric Corporation, Tokyo, Japan) mounted to an upright Eclipse FN1 microscope

equipped with a 60× 1.0 NA CFI Fluor lens (Nikon Instruments Inc., NY, USA). The GCaMP3 Ca^{2+} indicator expressed in ICC was excited at 488 nm using a laser coupled to a Borealis system (ANDOR Technology, Belfast, UK) to increase laser intensity and uniformity. The fluorescence emission (>515 nm) was captured using a high-speed EMCCD Camera (Andor iXon Ultra; ANDOR Technology). Pixel size using this acquisition system was 0.225 μm. Image sequences were collected at 33 fps using NIS-Elements (Nikon Instruments Inc.). All experiments were performed in the presence of nicardipine (100 nM) to minimize movements resulting from contractions.

ICC-DMP show low expression of Ca^{2+} channels that are highly sensitive to dihydropyridines (*Cacna1c*), although expression of *Cacna1d* was detected (Chen *et al.* 2007*a*). The concentration of nicardipine used to stabilize movements during imaging should have had minimal effects on the voltage-dependent Ca^{2+} channels encoded by *Cacna1d* (CaV 1.3 channels) (Xu & Lipscombe, 2001). However, control experiments were performed to test the possible involvement of these channels in regulating Ca^{2+} transients in ICC-DMP. Ca^{2+} transients were compared in the presence of 100 nM with events recorded after the addition of 3 μM or 10 μM nicardipine. Increasing nicardipine concentrations caused no detectable change in spontaneous Ca^{2+} transient frequency or patterns. We also tested the effects of elevated external $[K^+]$ (60 mM) with respect to causing general depolarization of the muscles. High $[K^+]_o$ had no effect on Ca^{2+} transients, supporting the idea that these events are not regulated by voltage-dependent mechanisms (data not shown). These controls suggested that inclusion of the low concentration of nicardipine to stabilize movements in our experiments probably did not affect the spontaneous Ca^{2+} transients of ICC-DMP.

The frequency and amplitude of Ca^{2+} signals measured with GCaMP3 are comparable with those measured using traditional fluorescent Ca^{2+} indicators (Ledoux *et al.* 2008; Kaestner *et al.* 2014). For example, the dissociation constant (K_D) value for Fluo 4 is ~345 nM and the K_D for GCaMP3 is in the same range (~340–600 nM) (Gee *et al.* 2000; Tian *et al.* 2009). GCaMP3 has greater affinity for Ca^{2+} than Fluo 4, as reflected by their Hill coefficients, 2.1–2.5 for GCaMP3 (Rose *et al.* 2014) and 1.4 for Fluo 4 (Gee *et al.* 2000), providing better signal-to-noise ratios and a broader range of Ca^{2+} measurement.

Calcium event analysis

Movies of Ca^{2+} activity in ICC-DMP were converted to a stack of Tiff images and were imported into either Image J, version 1.40 (National Institutes of Health, MD, USA) for Ca^{2+} event analysis or custom software (Volumetry G8c; GW Hennig, Department of Physiology & Cell Biology, University of Nevada School of Medicine, Reno, NV) for further analysis. Where necessary, tissue movement was stabilized to ensure accurate measurement of Ca^{2+} transients from identified cells.

ST maps. ST maps presented in the results were generated by rotating image stacks so that ICC-DMP were oriented vertically. Single cells from the FOV were masked using a flood-fill routine and ST maps of Ca^{2+}-induced fluorescence changes (averaged across the diameter of the cell within the mask) were constructed. Ca^{2+}-induced fluorescence intensity was calculated as a signal-to-noise ratio (SNR) whereby the amplitudes of the brightest Ca^{2+} events were divided by the SD of the background preceding the event (minus 2–3 s). The $\log_{10}$ of this value was calculated and multiplied by 20 to standardize the SNR as decibels. Typically, small Ca^{2+} transients (≤2 × amplitude of background noise) had SNR values of between 10 and 20 dB, with robust Ca^{2+} transients (5–15 × the amplitude of background noise) having SNR values between 30 and 40 dB.

ST map analysis. To quantify the rate of occurrence, amplitude and spread (distance travelled) of Ca^{2+} events within cells, a single pixel line was drawn along the mid axis of individual ICC-DMP and, using the 'reslice' function in Image J, a pseudo linescan image was produced with distance along the cell (μm) on the vertical axis and time (s) on the horizontal axis. Basal fluorescence was obtained from areas of the cell displaying the most uniform and least intense fluorescence (F_0) (Sergeant *et al.* 2006) with parameters calculated from traces generated at particular points along the cell (Fig. 3). Histograms were constructed to better represent the variations in Ca^{2+} responses. For visual clarity, red lines were fit to the histograms using a spline function from Prisim6 (GraphPad Software Inc. San Diego, CA).

ST map coincidence analysis. ST maps from adjacent ICC-DMP were coloured and overlaid to graphically display coincident Ca^{2+} transients in cells located orthogonally to each other. To quantify whether Ca^{2+} transients were co-ordinated in space and time, Ca^{2+} transients in the image stack were thresholded (>25 dB) and converted to Boolean particles to allow better analysis of shape and location. Ca^{2+} transient particles throughout the recording period were merged to show the overall position and time in which cells displayed active Ca^{2+} transients (transient min^{-1}) (Fig. 4*C*). Firing sites were identified by selecting only those particles that did not overlap with other particles in the previous frame of the movie. Merging the firing site particles throughout the recording period better shows the stability of location sites and their rate of occurrence (Ca^{2+} events min^{-1}) (Fig. 4*D*). To determine whether Ca^{2+} transient

firing sites in ICC-DMP were coincident in adjacent ICC-DMP, the distance and angle between firing sites within a time range (± 75 ms) was calculated throughout the entire recording period and plotted (Hennig *et al.* 2004). Frequency histograms were used to summarize the distribution of angles between firing sites (from parallel to perpendicular) within the time range. In long (4 min) recordings, traces of average Ca^{2+}-induced intensity were calculated from firing sites in individual ICC-DMP. Ca^{2+} transients were discriminated using maximum upstroke velocity (>9 IU s^{-1} in a 360 ms window). The number of coincident Ca^{2+} transients within a ± 66 ms time window was then calculated and plotted to determine whether synchronous firing between cells occurred; for example, see Fig. 6).

Statistical analysis

The occurrence of Ca^{2+} events was expressed as events fired per cell min^{-1}. The amplitude of Ca^{2+} events were expressed as $\Delta F/F_0$ and spatial spread was expressed as μm propagated per event. Statistical analysis was performed using either Student's *t*-test or a Mann–Whitney non-parametric test where appropriate. $P < 0.05$ was considered statistically significant. When describing data, *n* refers to the number of animals used in that dataset, whereas *c* refers to the numbers of cells used in that same data set.

Results

ICC-DMP expressing GCaMP3 were distributed normally and physiological responses attributed to ICC were intact in tamoxifen-treated mice

We first evaluated the expression of the Ca^{2+} biosensor (GCaMP3) to determine whether it was expressed specifically in ICC and whether the majority of ICC-DMP expressed GCaMP3. Immunohistochemical analysis using antibodies against GFP and c-Kit was performed on jejunal whole mount preparations from Kit-Cre-GCaMP3 mice. Cells with GFP (GCaMP3) immunoreactivity in the DMP region were present at an average density of 267 ± 17 cells mm^{-2} (n = 15) and there was an average minimum separation between cell bodies of 27.4 ± 1.9 μm (n = 15 tissues; c = 75) (Fig. 1*A*). We found a high degree of co-expression of GFP and c-Kit in ICC-DMP (Fig. 1*A*–*C*). For example, in FOVs imaged at 40× (230 × 230 μm), there were 22.4 ± 1.1 GFP^+ cells and 25.6 ± 1.5 c-Kit^+ ICC-DMP. GFP^+ cells were 100% c-Kit^+, whereas 87.5% of c-Kit^+ cells were GFP^+ (12 FOV from the small intestines of three animals). Previous studies have shown that electrical slow waves and responses to enteric nerve stimulation, namely processes attributed to functional ICC, are intact in mice treated with tamoxifen (Klein *et al.* 2013). We recorded electrical slow wave activity from intestinal circular muscle cells of Kit-Cre-GCaMP3 mice in the present study to confirm the maintenance of normal electrical activity (Fig. 1*D*). The resting membrane potential averaged –66 ± 1.5 mV and slow waves averaged 23 ± 1.3 mV in amplitude, and occurred at a frequency of 32 ± 0.5 cycles min^{-1} (n = 24 cells from three animals). Spontaneous electrical activity and postjunctional neural responses (Fig. 1*E*) were also recorded and were similar to the activity reported previously (Ward *et al.* 1994).

Spontaneous Ca^{2+} transients in ICC-DMP

Confocal imaging revealed spontaneous Ca^{2+} transients occurring in ICC-DMP (Fig. 2*A*; see also Supporting information, Movie S1). The Ca^{2+} transients in ICC-DMP were discrete localized events that fired in an apparently

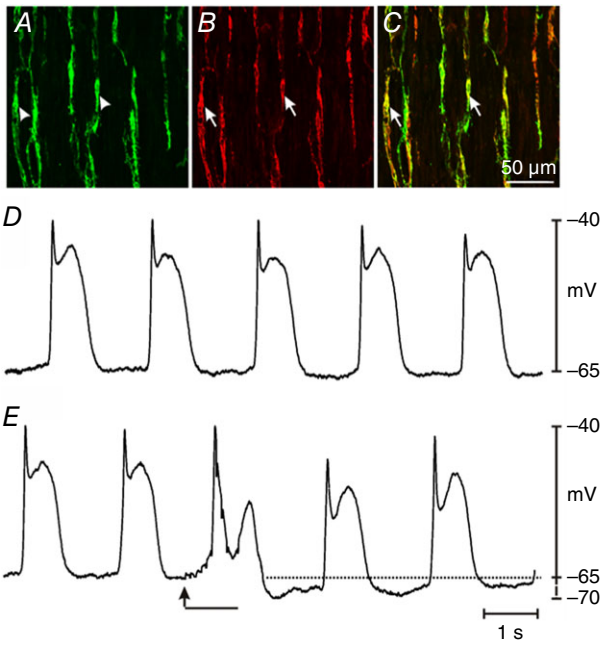

Figure 1. Kit-Cre-GCaMP3 was expressed in ICC-DMP and mice expressing the Ca^{2+} indicator displayed slow waves and responses to intrinsic nerve stimulation
A, digital reconstruction of a confocal image of GFP^+ cells at the level of the DMP region (arrowheads, green) in the jejunum. *B*, c-Kit^+ cells (i.e. identifying marker for ICC-DMP; arrows; red). *C*, merged image of *A* and *B* revealing co-localization of GFP and c-Kit (arrows; yellow). All c-Kit^+ cells expressed GFP (i.e. identifying expression of GCaMP3). The confocal images are digital reconstructions of single optical slices (1.0 μm in thickness). Scale bar in *C* applies to *A* to *C*. *D*, slow waves of normal amplitude and frequency recorded from a jejunal muscle strip from a Kit-Cre-GCaMP3 mouse. *E*, postjunctional responses to EFS (10 Hz; 0.5 ms duration pulses for 1 s; EFS initiated at the arrow for the duration of the solid black bar). EFS caused attenuation of slow waves immediately after initiation of stimulation and hyperpolarization, persisting for several seconds, after termination of EFS (dotted line).

stochastic manner along the entire length of cells under the basal conditions of our experiments (Fig. 2). Although many of the Ca^{2+} transients were restricted spatially, some developed into localized Ca^{2+} waves that propagated at velocities ranging from 34.67 to 235.5 μm^{-s} (mean = 93.6 ± 3.8 μm^{-s}) (Fig. 2).

The characteristics of Ca^{2+} transients in ICC-DMP during 30 s recording periods were evaluated in terms of rate of occurrence, amplitude, duration and spatial spread (Fig. 3*A*). Spontaneous Ca^{2+} transients occurred at between 12 to 376 events min^{-1} with an average of 124 ± 13 events min^{-1} ($c = 45$, $n = 16$). The amplitude of the Ca^{2+} transients ranged from 0.22 to 10.4 $\Delta(F/F_0)$ and averaged at 1.4 ± 0.02 $\Delta(F/F_0)$ ($c = 45$, $n = 16$) (Fig. 3*B*). Similarly, the durations of these events ranged from 30 to 900 ms at half-maximal amplitude (full duration half maximum) with a mean of 210 ± 2 ms ($c = 45$, $n = 16$) (Fig. 3*C*). The spatial spread of the Ca^{2+} transients showed a wide variation, from 0.3 to 57 μm, with an average distance of 8.4 ± 0.17 μm ($c = 45$, $n = 16$) (Fig. 3*D*).

Ca^{2+} transients in ICC-DMP arose from multiple sites along cells, as shown in Fig. 2 and 4*A–D*. The firing of these events appeared to be stochastic in nature. Although sites at various locations in the same cell fired together, there

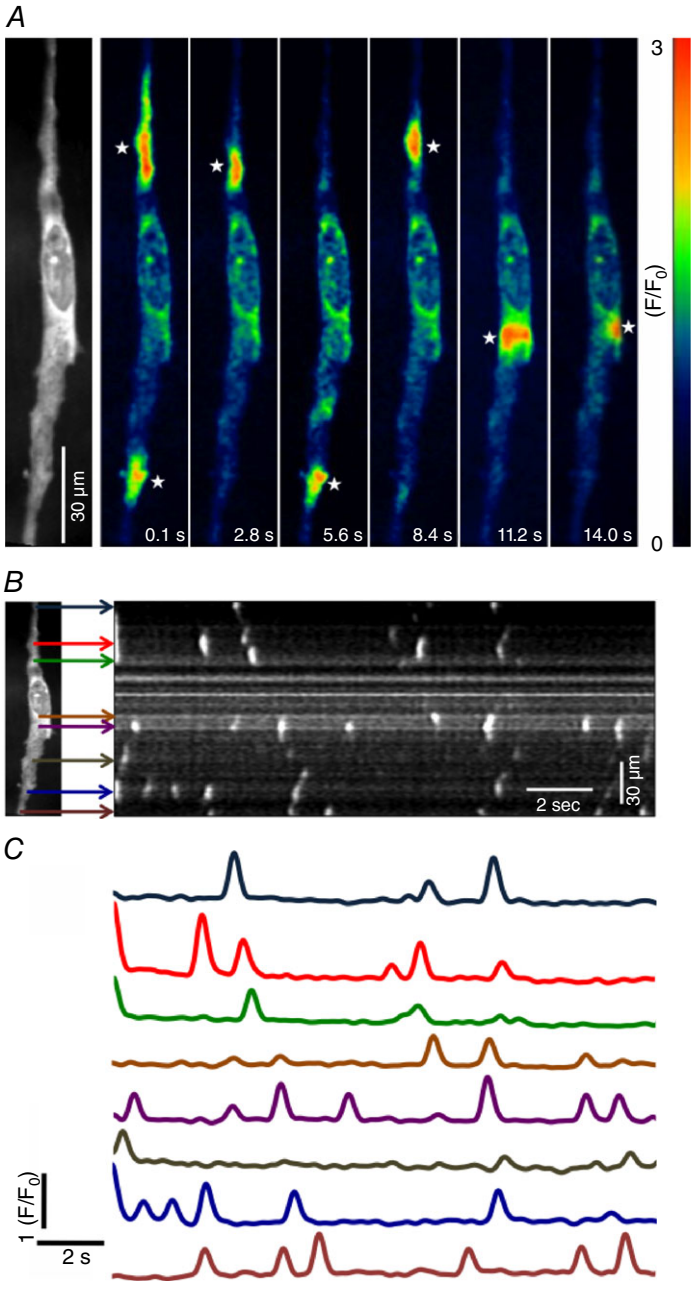

Figure 2. ICC-DMP generate spontaneous Ca^{2+} transients *in situ*
A, representative Ca^{2+} fluorescence intensity time-series images taken from a single ICC-DMP *in situ* (actual fluorescence image of the cell shown in the first panel). Images depict spontaneous Ca^{2+} transients occurring at different sites within the cell as a function of time. A colour-coded system was imported to depict fluorescence intensity (F/F_0). Low fluorescence areas are indictated in dark blue or black. High intensity fluorescence areas are indicated in red and orange. A colour calibration scale is provided in *A*. White stars indicate representative firing sites of Ca^{2+} in ICC-DMP. Scale bar in *A* is 30 μm. *B*, ST maps were generated to map the occurrence of Ca^{2+} events in single ICC-DMP. Coloured arrows indicate the discrete firing sites observed in a representative cell (one frame of a fluorescence image of the cell is shown to the left in *B*). *C*, plots of Ca^{2+} transients at each firing site during a 15 s recording period. Colours of traces in *C* correspond to the firing sites indicated by the arrows of the same colours in the ST map (*B*).

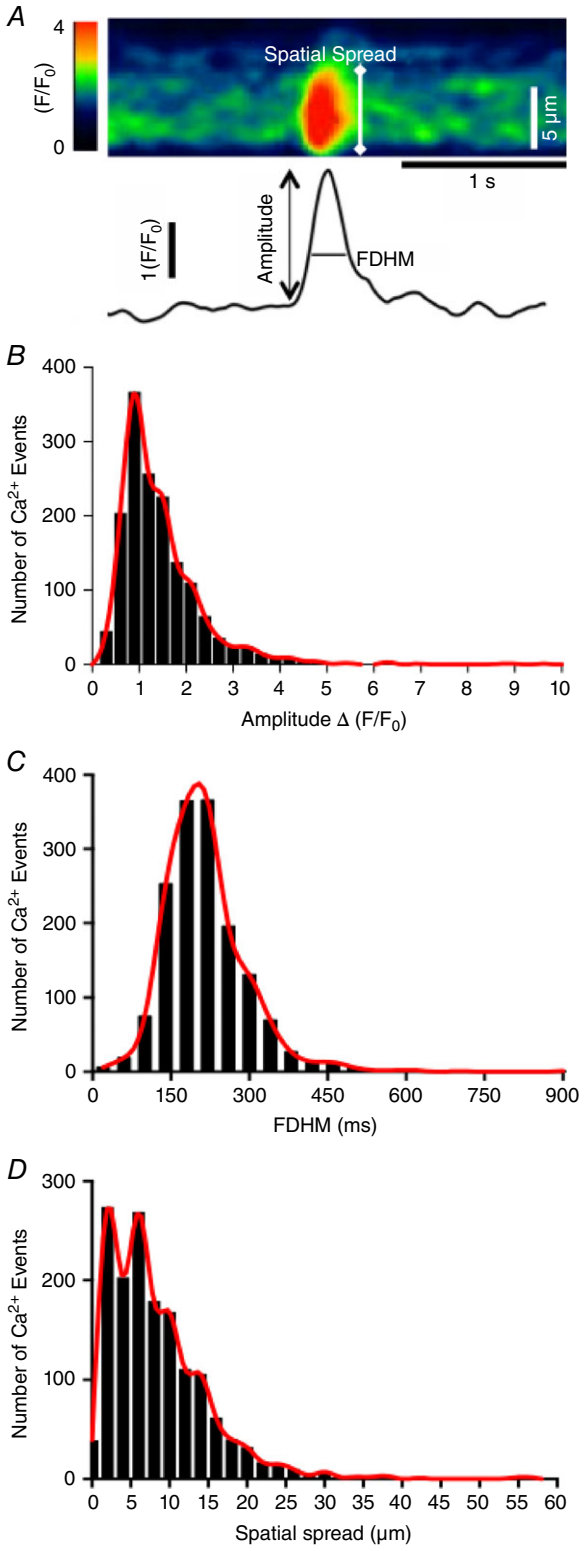

Figure 3. Analysis of Ca^{2+} transients in ICC-DMP
A, zoomed in portion of an ST map showing peak image of a single Ca^{2+} transient in an ICC-DMP and how the spatial spread of Ca^{2+} events was measured. Trace below image shows the Ca^{2+} transient plotted as a function of time and how amplitude and duration (full duration half maximum; FDHM) of Ca^{2+} transients were measured. *B–D*, histograms summarizing the range and distribution of Ca^{2+} transient amplitude (*B*), duration (*C*) and spatial spread (*D*) for hundreds of Ca^{2+} transients observed in ICC-DMP ($n = 16$, $c = 45$). Red lines were fit to the histograms for clarity using a spline function from Prisim6. Comparisons between data sets were made using Mann–Whitney tests.

was poor correlation between the occurrence of discrete Ca^{2+} transients. Overlays of ST maps of Ca^{2+} transients in adjacent cells running parallel to each other showed few events to be synchronous (i.e. 7.25% of total Ca^{2+} transients during a 30 s recording period; denoted as areas in cell images with combination colours; Fig. 4*B*). Coincidence analysis showed poor synchronicity of Ca^{2+} transients in single ICC-DMP and in adjacent ICC-DMP under basal conditions (Fig. 4*C–F*). Calculation of the distance and angle between the centroids of the firing sites for Ca^{2+} transients showed a higher incidence of firing sites in the parallel to the overall angle of cells in the FOV (i.e. sites within the same cell) compared to other angles (i.e. firing sites in adjacent cells) (Fig. 4*F*). The number of firing sites that were coincident at 75–90° (perpendicular) was around one-fifth (21%) of those counted at 0–15° (parallel) (Fig. 4*F*). This analysis suggests that Ca^{2+} transients in ICC-DMP were unable to be entrained or to propagate cell-to-cell.

Neuronal control over ICC-DMP

We examined whether the Ca^{2+} transients in ICC-DMP are regulated by basal neural activity. TTX (1 μM) applied to jejunal preparations almost doubled the rate of occurrence of Ca^{2+} transients from 82.9 ± 10.4 min^{-1} to 151.3 ± 20 min^{-1} ($n = 6$, $c = 22$, $P = 0.01$) (Fig. 5*A–C*). There was no significant change in the amplitudes ($P = 0.89$, $n = 6$, $c = 22$) (Fig. 5*D*), durations ($P = 0.41$, $n = 6$, $c = 22$; data not shown) and spatial spread ($P = 0.51$, $n = 6$, $c = 22$) (Fig. 5*E*) of Ca^{2+} transients in the presence of TTX. The significant increase in the occurrence of Ca^{2+} transients in the presence of TTX suggests that these events in ICC-DMP are tonically inhibited by the release of neurotransmitters known to suppress the activity of GI muscles (i.e. tonic inhibition) in some species (Wood, 1972; Lyster *et al.* 1995).

To confirm the ability and sensitivity of GCaMP3 to detect elevations in Ca^{2+} in ICC-DMP above basal levels and levels occurring during localized Ca^{2+} transients, we made brief applications of caffeine (10 mM). Caffeine rapidly elicited a global Ca^{2+} rise and increased the basal Ca^{2+} level throughout ICC-DMP. The increase in fluorescence amplitude in response to caffeine was ~3.5-fold above basal conditions (Fig. 5*F* and *G*).

We also evaluated whether there was rhythmic modulation in the firing of spontaneous Ca^{2+} transients

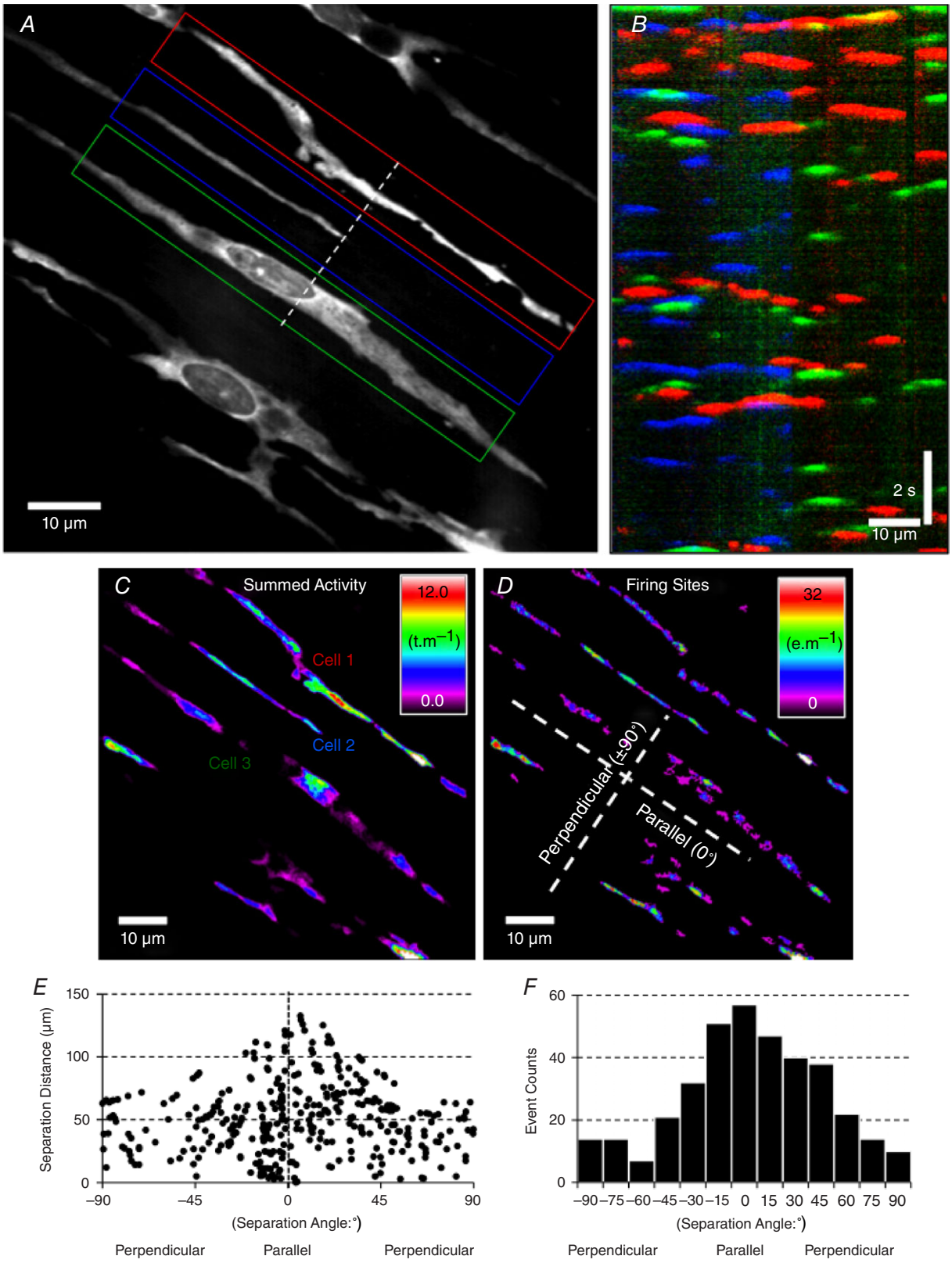

Figure 4. Asynchronous, stochastic nature of Ca^{2+} transients in ICC-DMP
A, a single frame of Ca^{2+} fluorescence in several ICC-DMP within a single FOV during a 15 s recording. Three adjacent cells (coded as red, blue and green regions of interest; ROIs) were selected and ST maps of the average

Ca^{2+} fluorescence intensity across the diameter of the cell were constructed. ST maps from each cell were colour coded to correspond to the red, blue and green cells and combined into a summed ST map in *B*. Coincidence of intracellular Ca^{2+} transients (at 90° to each other), coded as yellow, cyan and magenta areas, was minimal (i.e. less than 7.25%), indicating little spatial or temporal synchronization of Ca^{2+} transients in adjacent cells. *C*, prevalence and location of all Ca^{2+} transient particles (see Methods) in ICC-DMP within a FOV displayed as a heat map. *D*, Ca^{2+} transient firing sites were used to evaluate the coincidence of all Ca^{2+} events in ICC-DMP within the FOV. *E*, the separation angle and distance between Ca^{2+} events in ICC-DMP was measured and plotted, demonstrating that Ca^{2+} transients in single cells have a greater possibility of being coincident than events in adjacent cells (angles other than ∼0°). *F*, frequency histogram of the coincidence of Ca^{2+} transients is plotted in *E*.

in ICC-DMP during longer recording periods in the presence of TTX 1 μM (4 min continuous recordings at 33 fps, $n = 4$) (Fig. 6; see also Supporting information, Movie S2). No regular rhythmic modulation or oscillations in the amplitude or number of Ca^{2+} transients were noted in ICC-DMP within the FOVs (Fig. 6). Coincidence of firing of Ca^{2+} transients in ICC-DMP in the FOV was constant during these long periods of recordings, as indicated by the steady overall average of 10–20% of cells firing at any given time point ($n = 4$) (Fig. 6*E*). We also measured the overall area of Ca^{2+} transients (>25 dB) in ICC-DMP in the whole FOV (Fig. 6*F*). Although propagating events in one or more cells gave rise to periodic increases in overall Ca^{2+} transient area, these occurred at a rate similar to spontaneous firing of individual ICC-DMP and were constant throughout the 4 min recordings.

Ca^{2+} source(s) required for the generation of the spontaneous Ca^{2+} transients in ICC-DMP

We examined contributions from extracellular and intracellular Ca^{2+} sources on spontaneous Ca^{2+} transients in ICC-DMP. These experiments were performed in the presence of TTX to eliminate pre-junctional effects on the basal neuronal regulation observed in the experiments above.

Extracellular Ca^{2+} is not directly involved in the generation of spontaneous Ca^{2+} transients. To test the dependence of spontaneous Ca^{2+} transients on extracellular Ca^{2+}, KRB solution was replaced by KRB with no Ca^{2+} (i.e. nominally Ca^{2+}-free solution; Fig 7, with the same cell shown in Fig. 5). After a 12 min exposure to nominally Ca^{2+} free solution, there was no significant change in the rate of occurrence of Ca^{2+} transients (i.e. 43.3 ± 9.6 min^{-1} in Ca^{2+} free conditions compared to 50.5 ± 7.6 min^{-1} ($P = 0.57$, $n = 5$, $c = 12$) (Fig. 7*C*). Similarly, there was no significant change in the amplitude ($P = 0.4$, $n = 5$, $c = 12$) (Fig. 7*D*), duration ($P = 0.81$, $n = 5$, $c = 12$; data not shown) or spatial spread ($P = 0.76$, $n = 5$, $c = 12$) (Fig. 7*E*) of Ca^{2+} transients. These data suggest that spontaneous Ca^{2+} transients in ICC-DMP are not immediately dependent upon Ca^{2+} influx mechanisms and may be related to release of Ca^{2+} from intracellular stores.

Intracellular Ca^{2+} sources are responsible for the generation of spontaneous Ca^{2+} transients. 2-APB (100 μM) abolished spontaneous Ca^{2+} transients in ICC-DMP ($P = 0.001$; $n = 5$, $c = 11$) (Fig. 8*A–E*). Because of non-specific effects attributed to 2-APB (Bilmen *et al.* 2002; Bootman *et al.* 2002), we also tested another potent and membrane-permeant inhibitor of the $InsP_3$ receptors, XeC (1 μM). XeC reduced the occurrence of spontaneous Ca^{2+} transients from 78.9 ± 9 min^{-1} to 45.25 ± 10.1 min^{-1} ($P = 0.04$, $n = 4$, $c = 14$) (Fig. 8*F–H*). The amplitude ($P = 0.01$, $n = 4$, $c = 14$) (Fig. 8*I*), duration ($P = 0.044$, $n = 4$, $c = 14$) and spatial spread ($P = 0.01$, $n = 4$, $c = 14$) (Fig. 8*J*) were also inhibited significantly by XeC. XeC (10 μM) caused a greater degree of inhibition of all parameters of Ca^{2+} transients ($P = 0.001$, $n = 3$, $c = 10$) (Fig. 8*H–J*).

The ryanodine receptor (RyR) blocker, ryanodine (50 μM) (Fig. 9*C–E*) had no significant effect on the rate of occurrence ($P = 0.6$, $n = 4$, $c = 15$) (Fig. 9*C*), amplitude ($P = 0.21$, $n = 4$, $c = 15$) (Fig 9*D*), duration ($P = 0.63$, $n = 4$, $c = 15$) or spatial spread ($P = 0.73$, $n = 4$, $c = 15$) (Fig. 9*E*) of spontaneous Ca^{2+} transients. However, despite the lack of statistical significance, a trend of enhanced activity was observed with ryanodine (50 μM). At lower concentrations, ryanodine may act as an activator of RyRs (Serysheva II, 1998; Bootman *et al.* 2001). Therefore, we used a higher concentration of ryanodine (100 μM) and found almost complete abolition of spontaneous Ca^{2+} transients ($P = 0.001$, $n = 4$, $c = 14$) (Fig. 9*A–C*). A reduced amplitude ($P = 0.001$, $n = 4$, $c = 14$) (Fig. 9*D*), duration ($P = 0.001$, $n = 4$, $c = 14$;) and spatial spread of the remaining Ca^{2+} transients was also observed in the presence of RyR (100 μM; $P = 0.001$, $n = 4$, $c = 14$) (Fig. 9*E*).

Expression of ER Ca^{2+} channels (RyR and $InsP_3R$) in ICC

The results reported above suggest that both RyR and $InsP_3R$ contribute to the spontaneous Ca^{2+} release events in ICC-DMP. Recent electrophysiological studies have also shown that both Ca^{2+} release mechanisms contribute to STICs in ICC from the small intestine (Zhu *et al.* 2015), although the isoforms expressed in ICC were not determined. *Iptr1*, *Iptr2* and *Iptr3* were reported to be expressed in small intestinal muscles (Fujino *et al.* 1995)

and, similarly, RyRs (*Ryr1*, *Ryr2 and Ryr3)* were reported in GI muscles (Giannini *et al.* 1995; Aoyama *et al.* 2004; Morel *et al.* 2004). In the present study, we sorted ICC (CopGFP-Kit^+ cells) by FACS from small intestine muscles of $Kit^{+/copGFP}$ mice, as described previously (Peri *et al.* 2013), and characterized the expression of transcripts encoding RyR and $InsP_3R$ isoforms. We observed higher expression of *Ryr2* in ICC compared to other isoforms *Ryr1* and *Ryr3* (*Ryr1:* 0.0027 ± 0.0003; *Ryr2:* 0.014 ± 0.001; *Ryr3:* 0.0009 ± 0.0001, $P = 0.001$, $n = 4$) (Fig. 9*F*). We also found higher expression of *Itpr1* compared to *Itpr2* in ICC (*Itpr1:* 0.066 ± 0.01 *vs.* *Itpr2:* 0.01 ± 0.001, $P = 0.001$,

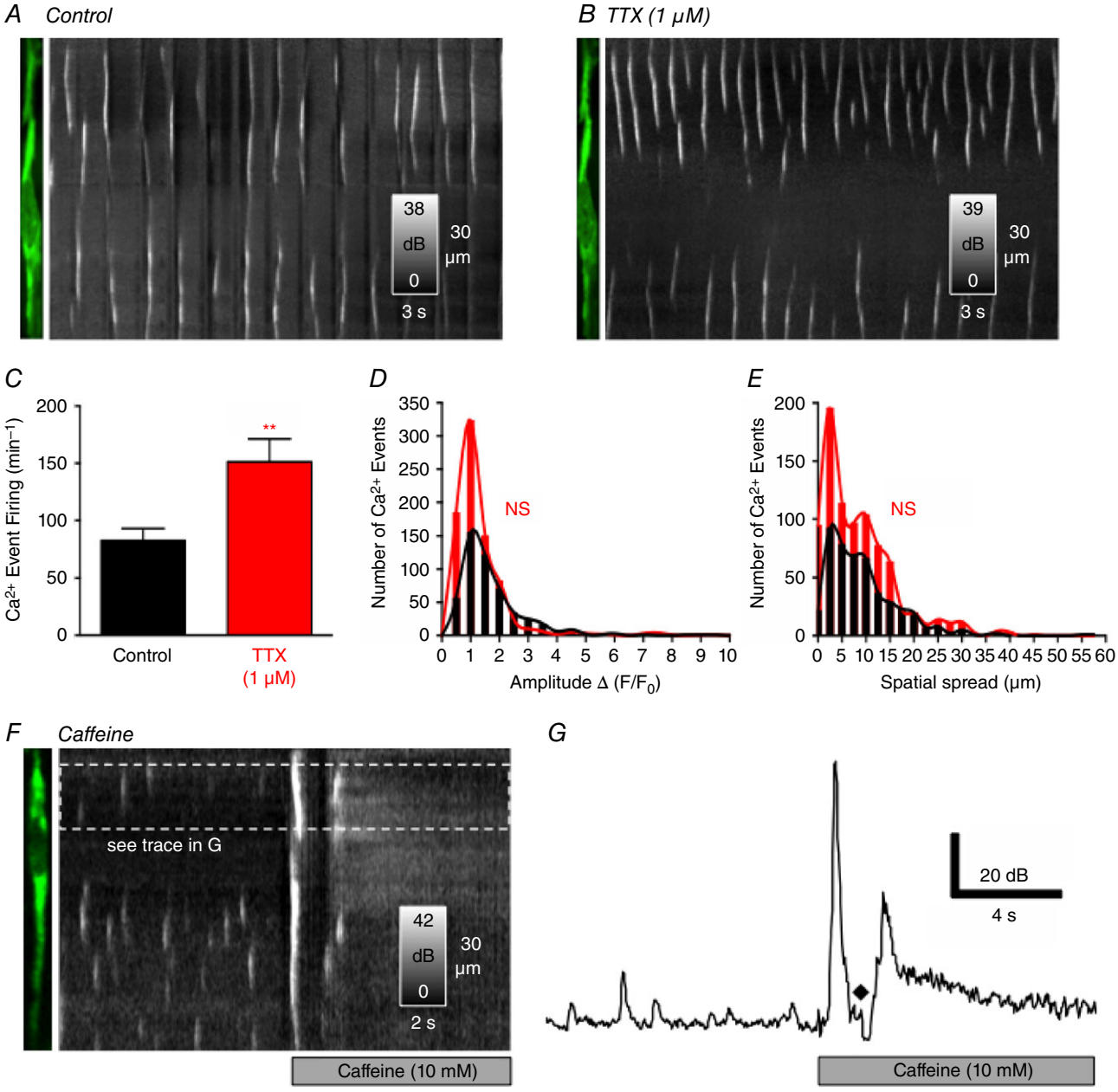

Figure 5. Effects of intrinsic neural inputs on Ca^{2+} transients in ICC-DMP
A, representative image of an ICC-DMP and ST map showing spontaneous Ca^{2+} transients in the ICC-DMP under control conditions (KRB perfusion of bath). *B*, application of TTX (1 μM) enhanced the occurrence of Ca^{2+} transients in the same ICC-DMP, as shown in the ST map. *C*, summary data showing the increase in Ca^{2+} transients after the addition of TTX (**$P = 0.01$, $n = 6$). *D*, summary histograms showing the amplitudes of Ca^{2+} transients (in presence of TTX; red bars and line) compared to control conditions (black bars and line; $P = 0.89$, $n = 6$). *E*, summary histograms of the spatial spread of Ca^{2+} transients in the presence of TTX compared to control ($P = 0.51$, $n = 6$). *F*, application of caffeine (10 mM) elicited a global Ca^{2+} fluorescence rise throughout ICC-DMP, as shown in the ST map, and the representative plot in *G* (♦) indicates a motion/focus artefact.

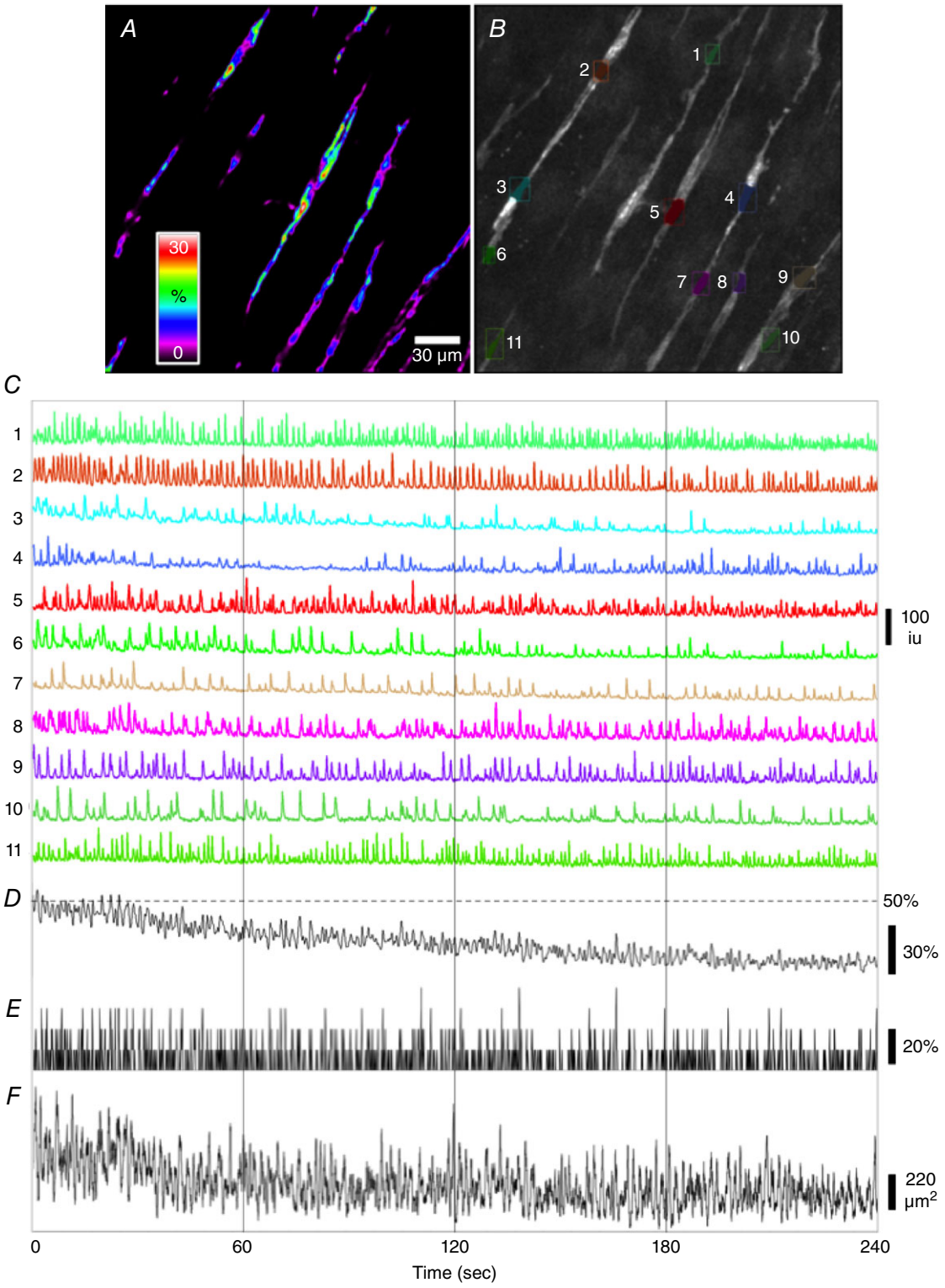

Figure 6. Firing pattern of spontaneous Ca^{2+} transients in ICC-DMP during long recording periods
A, image of the occurrence of active Ca^{2+} transients in ICC-DMP during a 4 min recording displayed as a heat map. Spectrum bar shows the percentage of overall recording time that sites were active. *B*, image showing a selection of ROIs of active Ca^{2+} transient firing sites in each ICC-DMP (coloured ROIs, as indicated by numbers 1 to 11 in the FOV) that were used to extract changes in Ca^{2+}-induced fluorescence changes in every cell. *C*, traces of Ca^{2+} transients plotted as a function of time from each ICC-DMP (coloured ROIs) in the FOV shown in *B*. *D*,

shows an averaged trace of all of the Ca^{2+} transients in *C*; the amplitude of each trace was normalized between 0–100% before averaging. *E*, trace of the number of cells that fired at each time point during a 4 min recording (within ± 66 ms time window; see Methods). The coincidence of Ca^{2+} transients firing between ICC-DMP in FOV over 4 min recordings was steady and did not show subminute fluctuations. The scale bar represents the total number of cells that fired Ca^{2+} transients within a ± 66 ms window over the 4 min recording period. *F*, trace of the overall area displaying active Ca^{2+} transients in all ICC-DMP in the FOV, per frame, after the movie was differentiated (>25 dB/Δt = 0.5 s). Spikes in the trace coincided with propagating Ca^{2+} transients. Again, by this analysis, no subminute oscillations in the overall firing patterns in ICC-DMP of four tissues (n = 4) were observed.

n = 4) (Fig. 9*G*) and did not resolve expression of the *Itpr3* subtype in ICC. The results demonstrate the dominant expression of *Itpr1* and *Ryr2* transcripts in ICC, and also show that ICC express several isoforms of Ca^{2+} release channels.

Role of the sarco/endoplasmic reticulum Ca^{2+}ATPases (SERCA) pump

Ca^{2+} store filling mechanisms provided by SERCA are important regulators of Ca^{2+} homeostasis and signalling in ICC from several organs (Hashitani & Suzuki, 2007; Dixon *et al.* 2011; Zhu *et al.* 2015). Therefore, we examined the role of the SERCA pump in generating Ca^{2+} transients in ICC-DMP using two well known antagonists of SERCA: thapsigargin (10 μM) and CPA (10 μM) (Fig. 10*A–C*). Application of either thapsigargin (n = 5, c = 17) (Fig. 10*D–F*) or CPA (n = 5, c = 12) (Fig. 10*D–F*) abolished the spontaneous Ca^{2+} transients in ICC-DMP. These results suggest that intact Ca^{2+} stores are essential for the spontaneous nature of Ca^{2+} transients in ICC-DMP and also that SERCA pumps are necessary for maintaining and refilling these stores.

Discussion

In the present study, we characterized and quantified the spontaneous Ca^{2+} transients generated in ICC-DMP

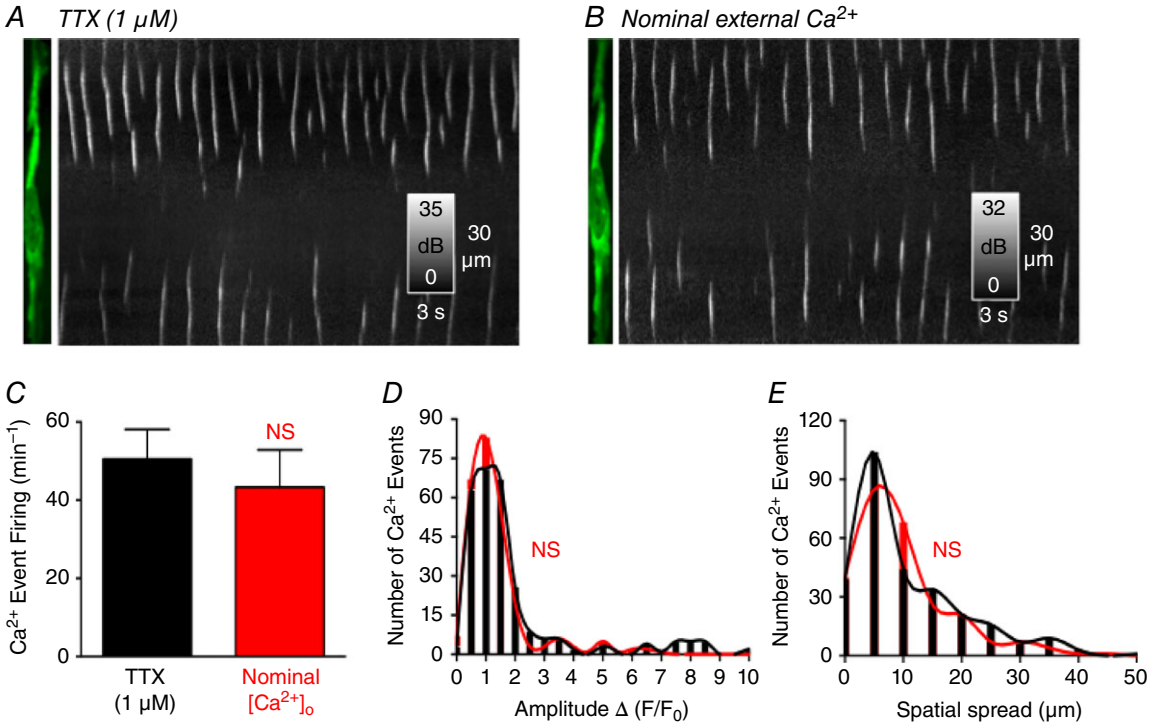

Figure 7. Effects of nominal extracellular Ca^{2+} on Ca^{2+} transients in ICC-DMP
A, representative image of an ICC-DMP and ST map showing spontaneous Ca^{2+} transients in the ICC-DMP in the presence of TTX and after the addition of nominally Ca^{2+}-free KRB solution in *B*. Reducing extracellular Ca^{2+} did not significantly affect the occurrence of Ca^{2+} transients. *C*, summary data show that there was no significant (NS) change in the rate of occurrence of Ca^{2+} events in nominal Ca^{2+}-free KRB (P = 0.57, n = 5). *D*, summary histograms showing the amplitudes of Ca^{2+} transients in the presence of TTX (black bars and line) and after the addition of nominal Ca^{2+}-free KRB (red bars and line) (P = 0.4, n = 5). *E*, summary histograms showing the spatial spread of Ca^{2+} transients in the presence of TTX and after the addition of nominal Ca^{2+}-free KRB (P = 0.76, n = 5).

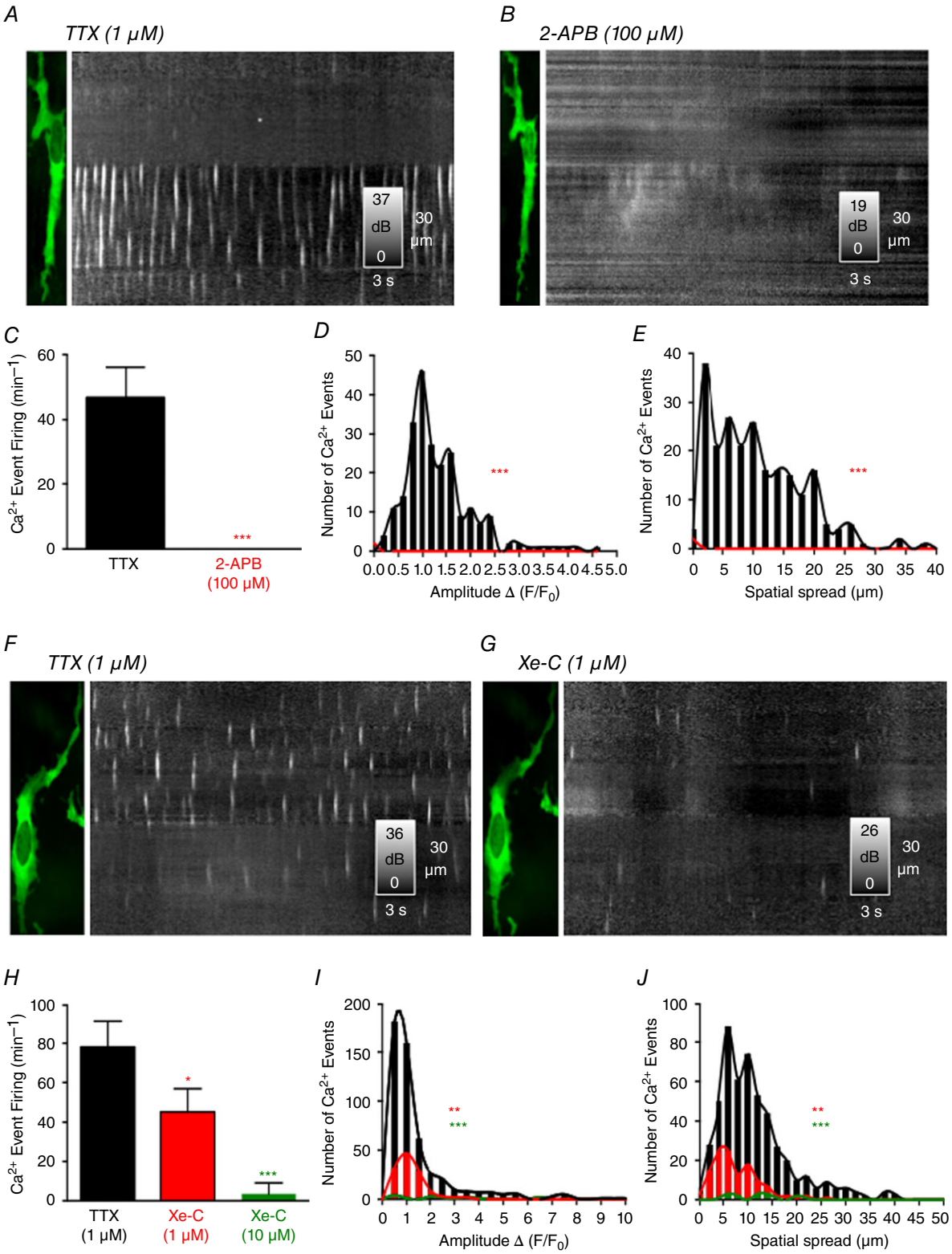

Figure 8. Effects of $InsP_3R$ inhibitors (2-APB and XeC) on ICC-DMP Ca^{2+} transients
A, image of ICC-DMP and ST map of Ca^{2+} transients in the presence of TTX. 2-APB (100 μM) blocked Ca^{2+} transients in ICC-DMP as shown in the ST map in *B*. *C*, summary data showing the inhibitory effects of 2-APB (100 μM) on the occurrence of Ca^{2+} transients (***$P = 0.001$, $n = 5$). *D*, comparison of amplitude histograms before (black bars and line) and after the addition of 2-APB (***$P = 0.001$, $n = 5$; red bars and line). Histograms

summarizing the spatial spread of Ca^{2+} transients before (black bars and line) and after the addition of 2-APB in *E* (***$P = 0.001$, $n = 5$; red bars and line). *F*, representative image of an ICC-DMP and an ST map of Ca^{2+} transients in the presence of TTX. XeC (1 μM) attenuated the occurrence of Ca^{2+} transients, as shown in the ST map in *G*. *H*, summary data showing the occurrence of Ca^{2+} transients in the presence of TTX and after the addition of XeC (1 μM and 10 μM; *$P = 0.04$, $n = 4$ and ***$P = 0.001$, $n = 3$, respectively). *I*, summary histograms showing the amplitudes of Ca^{2+} events in the presence of TTX (black bars and line) and in the presence of XeC (1 μM and 10 μM; red bars and line and green bars and line, respectively; **$P = 0.01$, $n = 4$ and ***$P = 0.001$, $n = 3$, respectively). *J*, summary histograms showing spatial spread of Ca^{2+} transients in the presence of TTX (black bars and line) and after the addition of XeC (1 μM and 10 μM; red bars and line and green bars and line, respectively; **$P = 0.01$, $n = 4$ and ***$P = 0.001$, $n = 3$, respectively).

of the small intestine *in situ*. This is the first study in which Ca^{2+} transients have been imaged in ICC using the Cre/loxP technology to accomplish cell-specific expression of a Ca^{2+} biosensor (GCaMP3). This approach allowed monitoring of Ca^{2+} transients in ICC with unprecedented resolution and without problematic interference from other cell types, such as occurs when membrane-permeant Ca^{2+} indicators are loaded into intact muscles. We found that the Ca^{2+} events in ICC-DMP differ significantly from the propagating events that have been recorded from ICC-MY in previous studies (Park *et al.* 2006; Lee *et al.* 2009). Ca^{2+} events in ICC-DMP were manifest as localized Ca^{2+} transients or Ca^{2+} waves with varying degrees of spatial spread. These events occurred in a stochastic manner. Our data suggest that spontaneous Ca^{2+} signalling in ICC-DMP is variable in terms of the rate of occurrence, amplitude, duration and spatial spread of Ca^{2+} transients. We found weak correlation between Ca^{2+} transients within single ICC-DMP and no correlation was found between events in nearby ICC-DMP. In long-term recordings (4 min), no evidence was found for low frequency Ca^{2+}oscillations in ICC-DMP that might result from 'phase coupling' with the slow waves generated by the ICC-MY population in the small intestine (Huizinga *et al.* 2014; Huizinga *et al.* 2015). Spontaneous Ca^{2+} transients in ICC-DMP were independent of Ca^{2+} entry pathways over the periods of our experiments and generated via Ca^{2+} release from intracellular stores via both $InsP_3$Rs and RyRs. Interdependence between $InsP_3$R and RyR is probable because blocking either channel severely diminished spontaneous Ca^{2+} transients. Our experiments also indicated that ICC-DMP are innervated, and the discharge of spontaneous Ca^{2+} transients was inhibited to some extent by ongoing neural input.

Functions of Ca^{2+} transients in ICC-DMP

In many cells, Ca^{2+} transients couple to Ca^{2+}-regulated ion channels in the plasma membrane (Nelson *et al.* 1995; ZhuGe *et al.* 1998; Wellman & Nelson, 2003). ICC of the small intestine express Ca^{2+}-activated Cl^- channels (CaCC; encoded by *Ano1*) (Hwang *et al.* 2009) and, to date, no other Ca^{2+}-regulated ion channels have been reported in cells isolated freshly from intestinal muscles. Therefore, it is probable that spontaneous Ca^{2+} transients observed in ICC-DMP initiate activation of STICs, and such events, recorded by the patch clamp technique, have been reported previously in these cells (Zhu *et al.* 2011). Measurements of electrical responses to Ca^{2+} transients were not obtained in the present study because neither direct impalement of ICC-DMP, nor patch clamp of any ICC, has been accomplished *in situ*. The fact that STICs display the same stochastic behaviour and have the same pharmacology as the Ca^{2+} transients is evidence, however, that these events are linked in ICC-DMP. Electrical coupling between ICC-DMP and smooth muscle cells (SMCs) (Komuro *et al.* 1999; Fujita *et al.* 2003) suggests that the Ca^{2+} transients in ICC-DMP produce an ongoing depolarizing (excitatory) influence on SMCs, and events corresponding to such activity (e.g. spontaneous transient depolarizations or 'unitary potentials') have been recorded in GI muscles and attributed to activity generated by ICC (Burns *et al.* 1996; Edwards *et al.* 1999; van Helden *et al.* 2000; Suzuki *et al.* 2003). There may be additional consequences of ongoing spontaneous Ca^{2+} transients in ICC that are not yet understood.

ICC-DMP as intermediaries in enteric motor neurotransmission

Considerable evidence suggests that ICC-IM (and ICC-DMP in the small intestine) are postjunctional targets for enteric neurotransmission, and these cells mediate, in part, responses to excitatory cholinergic and inhibitory nitrergic neurotransmission (Burns *et al.* 1996; Ward *et al.* 2000; Beckett *et al.* 2002; Suzuki *et al.* 2003; Ward *et al.* 2004; Ward & Sanders, 2006; Bhetwal *et al.* 2013; Klein *et al.* 2013; Sanders *et al.* 2014*a*). ICC-DMP also appear to contribute to neurokinin responses initiated by peptidergic motor neurons because they express NK1 receptors and internalize these receptors during nerve stimulation (Iino *et al.* 2004). Close associations between ICC-DMP and varicosities of motor neurons (Yamamoto, 1977; Ward, 2000; Ward & Sanders, 2001; Iino *et al.* 2004), expression of receptors and effectors involved in excitatory motor responses by ICC-DMP (Burns *et al.* 1996; Wang *et al.* 2003; Iino *et al.* 2004; Beckett *et al.* 2005; Chen *et al.* 2007*a*; Chen *et al.* 2007*b*), and gap junction coupling with

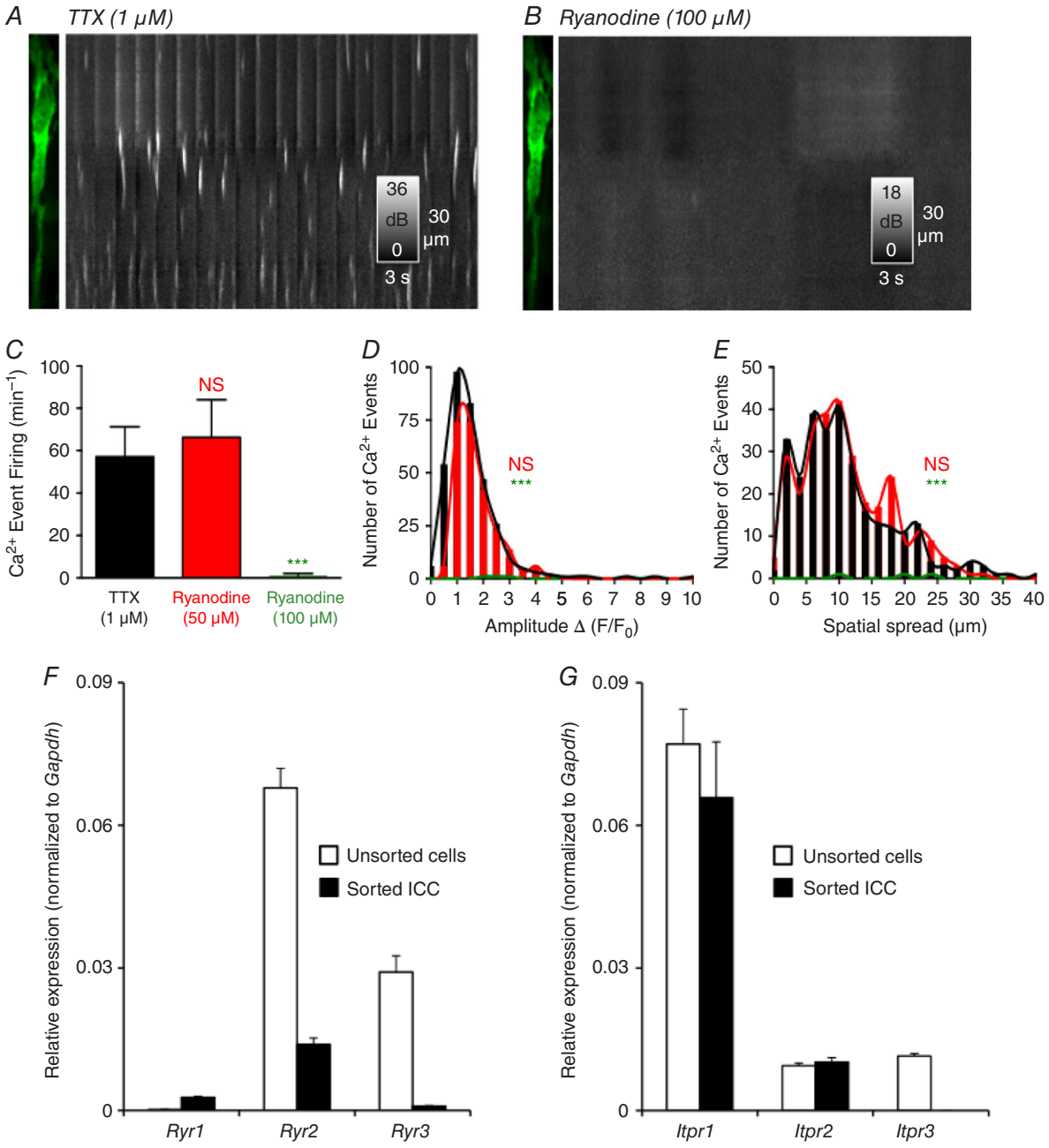

Figure 9. Effects of ryanodine on Ca^{2+} transients in ICC-DMP and molecular expression of RyR and $InsP_3R$ transcripts

A, image of ICC-DMP and ST map of Ca^{2+} transients in the presence of TTX (1 μM). *B*, ryanodine (100 μM) blocked Ca^{2+} transients in ICC-DMP as shown in the ST map. *C*, summary of occurrence of Ca^{2+} transients in the presence of ryanodine [50 μM; not significant (NS), $P = 0.6$, $n = 4$] and ryanodine (100 μM; $^{***}P = 0.001$, $n = 4$). *D*, histograms showing the amplitude of Ca^{2+} transients after the addition of ryanodine (50 μM; NS, $P = 0.7$, $n = 4$; red) or ryanodine (100 μM; green) compared to TTX alone ($^{***}P = 0.001$, $n = 4$). *E*, histograms showing the spatial spread of Ca^{2+} transients after the addition of ryanodine (50 μM; NS, $P = 0.3$, $n = 4$) and ryanodine (100 μM) compared to TTX ($^{***}P = 0.001$, $n = 4$). *F*, relative expression of RyR isoforms (*Ryr1*, *Ryr2*, *Ryr3*) in sorted ICC and in unsorted cells (i.e. mixed cell population after enzymatic dispersions of Jejunal muscles) as determined by qPCR. Transcripts of all three RyRs isoforms were resolved in sorted ICC; however, the highest isoform expressed in ICC was *Ryr2*. *G*, relative expression levels of $InsP_3R$ isoforms (*Itpr1*, *Itpr2*, *Itpr3*) in sorted ICC compared to unsorted cells. *Itpr1* was the highest isoform expressed in ICC. *Itpr3* expression was not resolved in ICC. The relative expression of each gene was normalized to the house-keeping gene, *Gapdh*. The data are plotted with SE bars and derived from experiments on four tissues of four animals that were dispersed and sorted separately, and then qPCR was performed on each individual sample.

smooth muscle cells (Mikkelsen *et al.* 1993; Park *et al.* 2006; Parsons & Huizinga, 2015) suggest a role for these cells in the integrated motor responses of the SMC/ICC/platelet derived growth factor receptor (PDGFR)α^{+} cell (SIP) syncytium.

The present study provides additional evidence of neural innervation and regulation of ICC-DMP. The neuronal blocker TTX enhanced spontaneous Ca^{2+} transients, suggesting ongoing neural regulation of Ca^{2+} transients. Because Ca^{2+} transients are probably coupled to activation of CaCC (see above), which would result in inward current, the ongoing neural input must be viewed as inhibitory. Thus, our findings suggest a role for ICC-DMP in participating in 'tonic inhibition' in the intestine, comprising behaviour in the GI tract that has been observed previously in many studies (Wood, 1972; Waterman & Costa, 1994; Spencer *et al.* 1998). Future studies will include a systematic investigation of the neurotransmitters and receptors that regulate Ca^{2+} transients in ICC-DMP and ICC-IM in other GI organs. Expression

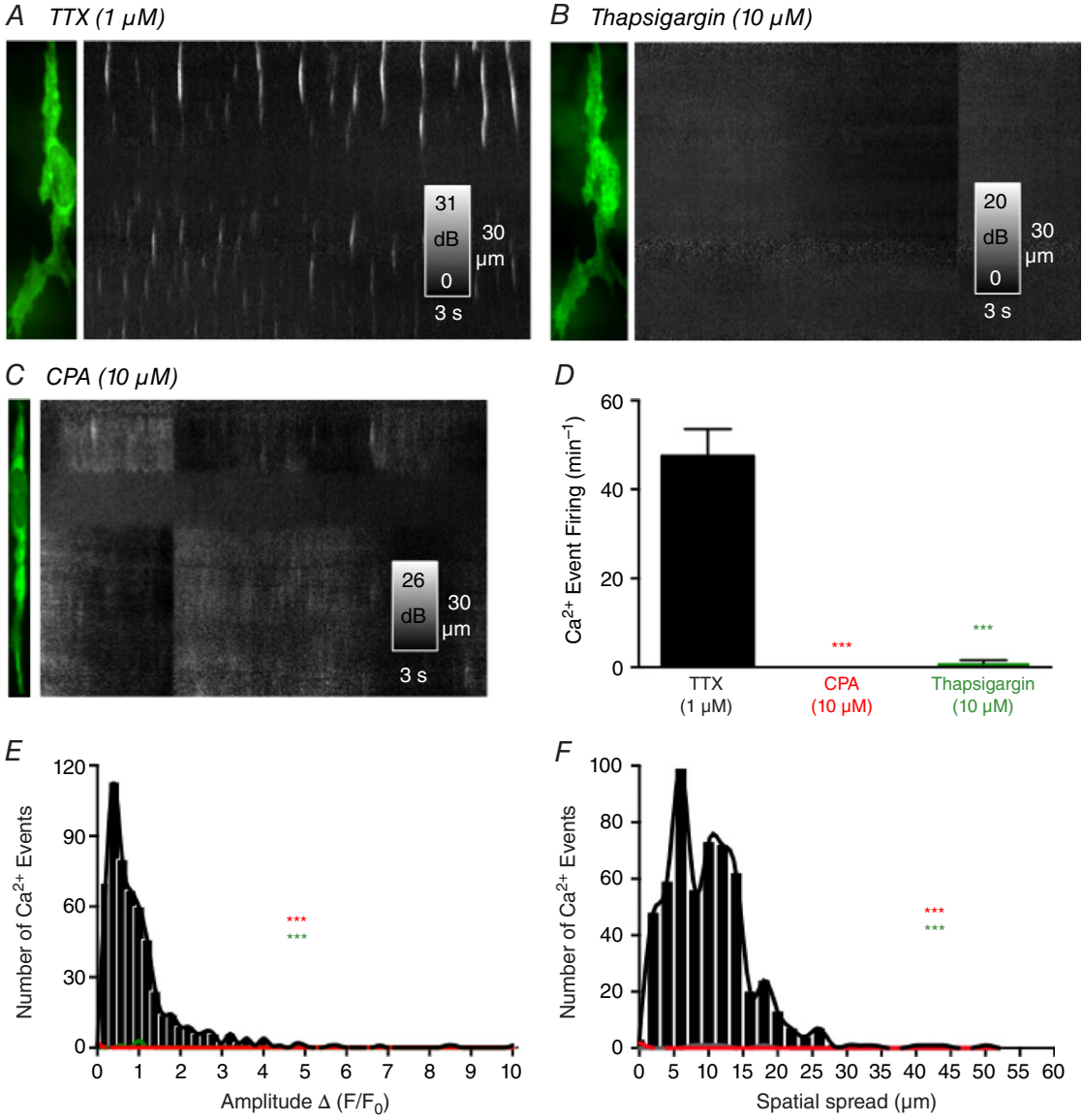

Figure 10. Effects of SERCA pump blockers on Ca^{2+} transients
A, ICC-DMP image and ST map of Ca^{2+} transients in the presence of TTX. Thapsigargin (10 μM) blocked Ca^{2+} transients as shown in the ST map in *B*. CPA (10 μM) also blocked Ca^{2+} transients in ICC-DMP. *C* and *D*, summary data showing the effects of SERCA pump inhibitors on Ca^{2+} transients (CPA: $^{***}P = 0.001$, $n = 5$; thapsigargin: $^{***}P = 0.001$, $n = 5$). *E* and *F*, histograms showing the amplitudes and spatial spreads of Ca^{2+} transients in the presence of TTX (black bars and line) and after the addition of CPA (both $^{***}P = 0.001$, $n = 5$; red bars and line) or thapsigargin (both $^{***}P = 0.001$, $n = 5$; green bars and line).

of genetically-encoded Ca^{2+} biosensors in ICC provides an unprecedented opportunity for determining the direct responsiveness of ICC *in situ* to several biological agonists (e.g. hormones, paracrine substances and inflammatory mediators).

No rhythmic modulation of Ca^{2+} events in ICC-DMP

Spontaneous Ca^{2+} transients arose from multiple sites along the length of ICC-DMP *in situ* and no correlation was found in the generation of events from site-to-site in cells. Furthermore, we found no evidence of synchronization between firing sites in adjacent ICC-DMP. By contrast, a recent study, attempting to determine the causes of segmental motor activity in the gut, reported that rhythmic low frequency Ca^{2+} oscillations are observed in ICC-DMP, and this oscillatory activity was suggested to 'phase-couple' to the higher frequency transients in ICC-MY resulting in segmentation patterns in the small intestine (Huizinga *et al.* 2014; Huizinga *et al.* 2015). It was also reported that most ICC-DMP are quiescent or display rhythmic Ca^{2+} activity that oscillated slowly at four cycles min^{-1}. Our observations contrast with these previous findings in that we observed ICC-DMP to fire localized Ca^{2+} transients in a non-rhythmic, stochastic manner, and we detected no synchronization of Ca^{2+} transients in multiple ICC-DMP, even during long periods of recording (4 min). ICC-MY were always present and slow waves were recorded in our muscle preparations (Fig. 1); however, we observed no apparent influence or modulation of the Ca^{2+} transients in ICC-DMP by the slow waves generated by ICC-MY. We suggest that both classes of ICC exert separate excitatory influences on SMCs of the small intestine through electrical coupling: (i) ICC-MY cause periodic depolarizations and increase the open probability of voltage-dependent Ca^{2+} channels that can lead to generation of Ca^{2+} action potentials in SMCs and (ii) ICC-DMP cause tonic regulation of the excitability of SMCs that would result from stochastic firing of Ca^{2+} transients and activation of STICs in thousands of ICC-DMP. Summation of STICs would provide a net depolarizing influence on the SIP syncytium and enhance the effectiveness of slow waves for generating Ca^{2+} action potentials and contraction.

For stable imaging, it was necessary to use a low concentration of nicardipine (100 nM) in our experiments. The reduction in movement from nicardipine is most probably the result of reduced voltage-dependent Ca^{2+} entry in SMCs and therefore a reduction in the ability of SMCs to fire Ca^{2+} action potentials. Although our findings suggest that there is no voltage-dependent regulation of the Ca^{2+} transients in ICC-DMP (e.g. elevating external $[K^+]$ and reducing the driving force for Ca^{2+} entry did not affect the Ca^{2+} transients), we cannot completely exclude the possibility that firing of Ca^{2+} action potentials in the adjacent SMCs electrically coupled to ICC-DMP, such as would occur in contracting small intestinal segments, has no effect on Ca^{2+} signalling in ICC-DMP. At present, imaging techniques, which require the maintenance of continuous focus, are unable to resolve changes in sub-cellular Ca^{2+} signalling that might occur during intense muscle movements.

Source of Ca^{2+} transients in ICC-DMP

Ca^{2+} transients in ICC-DMP appear to be a result of the release of Ca^{2+} from intracellular stores because Ca^{2+}-free external solution did not block these events. Inhibitors of Ca^{2+} uptake into ER stores with SERCA pump inhibitors blocked spontaneous Ca^{2+} transients, indicating the importance of functional stores in these events. Ca^{2+} release mechanisms from the stores may require synergism between $InsP_3Rs$ and RyRs because blockers of both channels significantly reduced or eliminated Ca^{2+} transients. Although a recent study on interstitial cells in the rabbit urethra has demonstrated that 2-APB acts preferentially on the $InsP_3R$ (Drumm *et al.* 2015), there have also been non-specific effects of 2-APB reported, such as inhibition of the SERCA pump and blockade of store-operated Ca^{2+} channels in the plasma membrane (Bootman *et al.* 2002; Peppiatt *et al.* 2003). Therefore, in the present study, we also tested a more selective $InsP_3R$ antagonist, XeC, and found significant attenuation of Ca^{2+} transients at 1 μM and complete inhibition at 10 μM. These findings are consistent with the effects of XeC on STICs in ICC, although the concentration required to block STICs in isolated cells was lower than the concentration necessary for abolishing Ca^{2+} transients *in situ* (Zhu *et al.* 2015). This may be a result of differences in drug penetration in single cells *vs.* intact muscles. We also found that RyRs contribute to generating Ca^{2+} transients in ICC-DMP. Initial experiments with 50 μM ryanodine did not significantly affect Ca^{2+} transients and, indeed, there was a small but not significant increase in activity. However, 100 μM ryanodine completely and irreversibly inhibited Ca^{2+} transients. Several studies have found dual actions of ryanodine at different concentrations. For example, at low concentrations (1–10 μM), ryanodine binding locks the RyRs into a long-lived subconductance state, whereas higher concentrations ($\sim$100 μM) irreversibly inhibit channel openings (Meissner & Henderson, 1987; Lai *et al.* 1989; McGrew *et al.* 1989; Serysheva II, 1998; Bootman *et al.* 2001). It has also been reported that oviduct muscle responses to ryanodine (50 μM) were associated with a depolarization of muscle membrane potential (Dixon *et al.* 2011). This is consistent with the effects of ryanodine observed in the present study because ryanodine at 50 μM slightly increased Ca^{2+} transients in ICC-DMP. Taken

together, our data indicate that both RyRs and $InsP_3Rs$ contribute synergistically to spontaneous Ca^{2+} signalling in ICC-DMP.

Nature of the ER channels in ICC

Spontaneous Ca^{2+} transients in ICC-DMP exhibited significant variation in their spatial size, amplitude and time course. It appears that Ca^{2+} events do not occur as clearly separate signals of specific durations and spread as might be observed in a quantal system. Instead, we observed both highly localized events and Ca^{2+} waves that propagated over varying distances within cells. This spectrum of Ca^{2+} behaviour was probably the result of ST recruitment of localized events, possibly occurring via a mechanism involving Ca^{2+}-induced Ca^{2+} release. Additionally, the interplay and mechanisms of activation between RyR and $InsP_3R$ may further complicate interpretations. In colonic smooth muscle cells, for example, it was shown that ryanodine could reduce $InsP_3$ mediated Ca^{2+} signals by directly affecting $InsP_3Rs$ or by depleting the shared store of Ca^{2+} (MacMillan *et al.* 2005). It is also known that RyRs and $InsP_3Rs$ can be arranged in clusters on the ER membrane, and variable numbers of channels with variable open states may constitute individual clusters (Jaggar *et al.* 2000). The variability in Ca^{2+} release dynamics in ICC-DMP may result from the release of clusters of Ca^{2+} channels of different size or molecular composition.

Another explanation for the variability in Ca^{2+} transients might come from heterogeneity in the distribution of subcellular release sites. To better understand this possibility, we examined the expression profile of $InsP_3Rs$ and RyRs in sorted ICC to identify the major types of ER Ca^{2+} channels in ICC. *Itpr1* transcripts were highly expressed in ICC, as suggested previously from microarray analysis (Chen *et al.* 2007*a*). However, *Itpr2* was also expressed in ICC and these channels might also contribute to the composition of $InsP_3Rs$ responsible for Ca^{2+} transients. RyRs were not resolved in the expression patterns noted in the previous microarray study (Chen *et al.* 2007*a*); however, we found expression of *Ryr2* and *Ryr1* in the current analysis by qPCR. These findings are in contrast to a previous study of cultured-clusters of gastric ICC in which *Ryr3* was the only isoform detected (Liu *et al.* 2005). Having multiple Ca^{2+} channels expressed in ICC makes it difficult to probe the nature of Ca^{2+} release mechanisms by use of genetic knockouts.

In summary, the present study demonstrates the stochastic nature and properties of Ca^{2+} transients in ICC-DMP of the murine small intestine. Ca^{2+} events in ICC-DMP are independent of events in other regions of the same cell and clearly independent of the events in adjacent cells. We found no evidence, even during relatively long periods of continuous recording, of co-ordination in the generation of Ca^{2+} transients between ICC-DMP or by responding to the activity of other cells, such as phase-coupling between ICC-MY and ICC-DMP (Huizinga *et al.* 2014). Taken together, observations from the present and previous studies suggest that Ca^{2+} transients in ICC-DMP couple to STICs as a result of activation of CaCC, and this activity provides a net depolarizing influence on the SIP syncytium in the small intestine. Basal activity of intrinsic motor neurons tends to suppress Ca^{2+} transients in ICC-DMP, thereby contributing to the tonic inhibition observed in GI muscles. Thus, the Ca^{2+} transients of ICC-DMP contribute to setting the basal excitability of intestinal muscles, and neural input during digestive states and reflexes may regulate muscle excitability by modulating Ca^{2+} release in ICC-DMP. The Ca^{2+} transients of ICC-DMP result from Ca^{2+} release from internal stores and appear to depend upon interactions between $InsP_3Rs$ and RyRs. Ca^{2+} entry does not appear to influence Ca^{2+} transients over the short term.

References

Aoyama M, Yamada A, Wang J, Ohya S, Furuzono S, Goto T, Hotta S, Ito Y, Matsubara T, Shimokata K, Chen SR, Imaizumi Y & Nakayama S (2004). Requirement of ryanodine receptors for pacemaker Ca^{2+} activity in ICC and HEK293 cells. *J Cell Sci* **117**, 2813–2825.

Baker SA, Hennig GW, Salter AK, Kurahashi M, Ward SM & Sanders KM (2013). Distribution and Ca($^{2+}$) signalling of fibroblast-like (PDGFR(+)) cells in the murine gastric fundus. *J Physiol* **591**, 6193–6208.

Baker SA, Hennig GW, Ward SM & Sanders KM (2015). Temporal sequence of activation of cells involved in purinergic neurotransmission in the colon. *J Physiol* **593**, 1945–1963.

Beckett EA, Horiguchi K, Khoyi M, Sanders KM & Ward SM (2002). Loss of enteric motor neurotransmission in the gastric fundus of Sl/Sl(d) mice. *J Physiol* **543**, 871–887.

Beckett EA, Takeda Y, Yanase H, Sanders KM & Ward SM (2005). Synaptic specializations exist between enteric motor nerves and interstitial cells of Cajal in the murine stomach. *J Comp Neurol* **493**, 193–206.

Bhetwal BP, Sanders KM, An C, Trappanese DM, Moreland RS & Perrino BA (2013). Ca^{2+} sensitization pathways accessed by cholinergic neurotransmission in the murine gastric fundus. *J Physiol.*

Bilmen JG, Wootton LL, Godfrey RE, Smart OS & Michelangeli F (2002). Inhibition of SERCA Ca^{2+} pumps by 2-aminoethoxydiphenyl borate (2-APB). 2-APB reduces both Ca^{2+} binding and phosphoryl transfer from ATP, by interfering with the pathway leading to the Ca^{2+}-binding sites. *Eur J Biochem* **269**, 3678–3687.

Blair PJ, Bayguinov Y, Sanders KM & Ward SM (2012). Interstitial cells in the primate gastrointestinal tract. *Cell Tissue Res* **350**, 199–213.

Bootman MD, Collins TJ, Mackenzie L, Roderick HL, Berridge MJ & Peppiatt CM (2002). 2-aminoethoxydiphenyl borate (2-APB) is a reliable blocker of store-operated Ca^{2+} entry but an inconsistent inhibitor of InsP3-induced Ca^{2+} release. *FASEB J* **16**, 1145–1150.

Bootman MD, Collins TJ, Peppiatt CM, Prothero LS, MacKenzie L, De Smet P, Travers M, Tovey SC, Seo JT, Berridge MJ, Ciccolini F & Lipp P (2001). Calcium signalling – an overview. *Semin Cell Dev Biol* **12**, 3–10.

Burns AJ, Lomax AE, Torihashi S, Sanders KM & Ward SM (1996). Interstitial cells of Cajal mediate inhibitory neurotransmission in the stomach. *Proc Natl Acad Sci USA* **93**, 12008–12013.

Chen H, Ordog T, Chen J, Young DL, Bardsley MR, Redelman D, Ward SM & Sanders KM (2007*a*). Differential gene expression in functional classes of interstitial cells of Cajal in murine small intestine. *Physiol Genomics* **31**, 492–509.

Chen H, Redelman D, Ro S, Ward SM, Ordog T & Sanders KM (2007*b*). Selective labeling and isolation of functional classes of interstitial cells of Cajal of human and murine small intestine. *Am J Physiol Cell Physiol* **292**, C497–C507.

Daniel EE & Posey-Daniel V (1984). Neuromuscular structures in opossum esophagus: role of interstitial cells of Cajal. *Am J Physiol Gastrointest Liver Physiol* **246**, G305–G315.

Dickens EJ, Hirst GD & Tomita T (1999). Identification of rhythmically active cells in guinea-pig stomach. *J Physiol* **514**, 515–531.

Dixon RE, Britton FC, Baker SA, Hennig GW, Rollings CM, Sanders KM & Ward SM (2011). Electrical slow waves in the mouse oviduct are dependent on extracellular and intracellular calcium sources. *Am J Physiol Cell Physiol* **301**, C1458–C1469.

Drumm BT, Large RJ, Hollywood MA, Thornbury KD, Baker SA, Harvey BJ, McHale NG & Sergeant GP (2015). The role of Ca influx in spontaneous Ca wave propagation in interstitial cells of Cajal from the rabbit urethra. *J Physiol* **593**, 333–3350.

Edwards FR, Hirst GD & Suzuki H (1999). Unitary nature of regenerative potentials recorded from circular smooth muscle of guinea-pig antrum. *J Physiol* **519**, 235–250.

Fujino I, Yamada N, Miyawaki A, Hasegawa M, Furuichi T & Mikoshiba K (1995). Differential expression of type 2 and type 3 inositol 1,4,5-trisphosphate receptor mRNAs in various mouse tissues: in situ hybridization study. *Cell Tissue Res* **280**, 201–210.

Fujita A, Takeuchi T, Jun H & Hata F (2003). Localization of Ca^{2+}-activated K^+ channel, SK3, in fibroblast-like cells forming gap junctions with smooth muscle cells in the mouse small intestine. *J Pharmacol Sci* **92**, 35–42.

Gee KR, Brown KA, Chen WN, Bishop-Stewart J, Gray D & Johnson I (2000). Chemical and physiological characterization of fluo-4 $Ca(^{2+})$-indicator dyes. *Cell Calcium* **27**, 97–106.

Giannini G, Conti A, Mammarella S, Scrobogna M & Sorrentino V (1995). The ryanodine receptor/calcium channel genes are widely and differentially expressed in murine brain and peripheral tissues. *J Cell Biol* **128**, 893–904.

Gomez-Pinilla PJ, Gibbons SJ, Bardsley MR, Lorincz A, Pozo MJ, Pasricha PJ, Van de Rijn M, West RB, Sarr MG, Kendrick ML, Cima RR, Dozois EJ, Larson DW, Ordog T & Farrugia G (2009). Ano1 is a selective marker of interstitial cells of Cajal in the human and mouse gastrointestinal tract. *Am J Physiol Gastrointest Liver Physiol* **296**, G1370–G1381.

Hashitani H & Suzuki H (2007). Properties of spontaneous Ca^{2+} transients recorded from interstitial cells of Cajal-like cells of the rabbit urethra in situ. *J Physiol* **583**, 505–519.

Hennig GW, Hirst GD, Park KJ, Smith CB, Sanders KM, Ward SM & Smith TK (2004). Propagation of pacemaker activity in the guinea-pig antrum. *J Physiol* **556**, 585–599.

Huizinga JD, Chen JH, Zhu YF, Pawelka A, McGinn RJ, Bardakjian BL, Parsons SP, Kunze WA, Wu RY, Bercik P, Khoshdel A, Chen S, Yin S, Zhang Q, Yu Y, Gao Q, Li K, Hu X, Zarate N, Collins P, Pistilli M, Ma J, Zhang R & Chen D (2014). The origin of segmentation motor activity in the intestine. *Nat Commun* **5**, 3326.

Huizinga JD, Parsons SP, Chen JH, Pawelka A, Pistilli M, Li C, Yu Y, Ye P, Liu Q, Tong M, Zhu YF & Wei D (2015). Motor patterns of the small intestine explained by phase-amplitude coupling of two pacemaker activities: the critical importance of propagation velocity. *Am J Physiol Cell Physiol* **309**, C403–C414.

Huizinga JD, Thuneberg L, Kluppel M, Malysz J, Mikkelsen HB & Bernstein A (1995). W/kit gene required for interstitial cells of Cajal and for intestinal pacemaker activity. *Nature* **373**, 347–349.

Hwang SJ, Blair PJ, Britton FC, O'Driscoll KE, Hennig G, Bayguinov YR, Rock JR, Harfe BD, Sanders KM & Ward SM (2009). Expression of anoctamin 1/TMEM16A by interstitial cells of Cajal is fundamental for slow wave activity in gastrointestinal muscles. *J Physiol* **587**, 4887–4904.

Iino S, Ward SM & Sanders KM (2004). Interstitial cells of Cajal are functionally innervated by excitatory motor neurones in the murine intestine. *J Physiol* **556**, 521–530.

Jaggar JH, Porter VA, Lederer WJ & Nelson MT (2000). Calcium sparks in smooth muscle. *Am J Physiol Cell Physiol* **278**, C235–C256.

Kaestner L, Scholz A, Tian Q, Ruppenthal S, Tabellion W, Wiesen K, Katus HA, Muller OJ, Kotlikoff MI & Lipp P (2014). Genetically encoded Ca^{2+} indicators in cardiac myocytes. *Circ Res* **114**, 1623–1639.

Klein S, Seidler B, Kettenberger A, Sibaev A, Rohn M, Feil R, Allescher HD, Vanderwinden JM, Hofmann F, Schemann M, Rad R, Storr MA, Schmid RM, Schneider G & Saur D (2013). Interstitial cells of Cajal integrate excitatory and inhibitory neurotransmission with intestinal slow-wave activity. *Nat Commun* **4**, 1630.

Komuro T, Seki K & Horiguchi K (1999). Ultrastructural characterization of the interstitial cells of Cajal. *Arch Histol Cytol* **62**, 295–316.

Lai FA, Misra M, Xu L, Smith HA & Meissner G (1989). The ryanodine receptor-Ca^{2+} release channel complex of skeletal muscle sarcoplasmic reticulum. Evidence for a cooperatively coupled, negatively charged homotetramer. *J Biol Chem* **264**, 16776–16785.

Langton P, Ward SM, Carl A, Norell MA & Sanders KM (1989). Spontaneous electrical activity of interstitial cells of Cajal isolated from canine proximal colon. *Proc Natl Acad Sci USA* **86**, 7280–7284.

Ledoux J, Taylor MS, Bonev AD, Hannah RM, Solodushko V, Shui B, Tallini Y, Kotlikoff MI & Nelson MT (2008). Functional architecture of inositol 1,4,5-trisphosphate signaling in restricted spaces of myoendothelial projections. *Proc Natl Acad Sci USA* **105**, 9627–9632.

Lee HT, Hennig GW, Park KJ, Bayguinov PO, Ward SM, Sanders KM & Smith TK (2009). Heterogeneities in ICC Ca^{2+} activity within canine large intestine. *Gastroenterology* **136**, 2226–2236.

Liu HN, Ohya S, Wang J, Imaizumi Y & Nakayama S (2005). Involvement of ryanodine receptors in pacemaker Ca^{2+} oscillation in murine gastric ICC. *Biochem Biophys Res Commun* **328**, 640–646.

Lowie BJ, Wang XY, White EJ & Huizinga JD (2011). On the origin of rhythmic calcium transients in the ICC-MP of the mouse small intestine. *Am J Physiol Gastrointest Liver Physiol* **301**, G835–G845.

Lyster DJ, Bywater RA & Taylor GS (1995). Neurogenic control of myoelectric complexes in the mouse isolated colon. *Gastroenterology* **108**, 1371–1378.

MacMillan D, Chalmers S, Muir TC & McCarron JG (2005). IP3-mediated Ca^{2+} increases do not involve the ryanodine receptor, but ryanodine receptor antagonists reduce IP3-mediated Ca^{2+} increases in guinea-pig colonic smooth muscle cells. *J Physiol* **569**, 533–544.

McGrew SG, Wolleben C, Siegl P, Inui M & Fleischer S (1989). Positive cooperativity of ryanodine binding to the calcium release channel of sarcoplasmic reticulum from heart and skeletal muscle. *Biochemistry* **28**, 1686–1691.

Meissner G & Henderson JS (1987). Rapid calcium release from cardiac sarcoplasmic reticulum vesicles is dependent on Ca^{2+} and is modulated by Mg^{2+}, adenine nucleotide, and calmodulin. *J Biol Chem* **262**, 3065–3073.

Mikkelsen HB, Huizinga JD, Thuneberg L & Rumessen JJ (1993). Immunohistochemical localization of a gap junction protein (connexin43) in the muscularis externa of murine, canine, and human intestine. *Cell Tissue Res* **274**, 249–256.

Morel JL, Rakotoarisoa L, Jeyakumar LH, Fleischer S, Mironneau C & Mironneau J (2004). Decreased expression of ryanodine receptors alters calcium-induced calcium release mechanism in mdx duodenal myocytes. *J Biol Chem* **279**, 21287–21293.

Nelson MT, Cheng H, Rubart M, Santana LF, Bonev AD, Knot HJ & Lederer WJ (1995). Relaxation of arterial smooth muscle by calcium sparks. *Science* **270**, 633–637.

Ordog T, Ward SM & Sanders KM (1999). Interstitial cells of Cajal generate electrical slow waves in the murine stomach. *J Physiol* **518**, 257–269.

Park KJ, Hennig GW, Lee HT, Spencer NJ, Ward SM, Smith TK & Sanders KM (2006). Spatial and temporal mapping of pacemaker activity in interstitial cells of Cajal in mouse ileum in situ. *Am J Physiol Cell Physiol* **290**, C1411–C1427.

Parsons SP & Huizinga JD (2015). Effects of gap junction inhibition on contraction waves in the murine small intestine in relation to coupled oscillator theory. *Am J Physiol Gastrointest Liver Physiol* **308**, G287–G297.

Peppiatt CM, Collins TJ, Mackenzie L, Conway SJ, Holmes AB, Bootman MD, Berridge MJ, Seo JT & Roderick HL (2003). 2-Aminoethoxydiphenyl borate (2-APB) antagonises inositol 1,4,5-trisphosphate-induced calcium release, inhibits calcium pumps and has a use-dependent and slowly reversible action on store-operated calcium entry channels. *Cell Calcium* **34**, 97–108.

Peri LE, Sanders KM & Mutafova-Yambolieva VN (2013). Differential expression of genes related to purinergic signaling in smooth muscle cells, PDGFRalpha-positive cells, and interstitial cells of Cajal in the murine colon. *Neurogastroenterol Motil* **25**, e609–e620.

Ro S, Park C, Jin J, Zheng H, Blair PJ, Redelman D, Ward SM, Yan W & Sanders KM (2010). A model to study the phenotypic changes of interstitial cells of Cajal in gastrointestinal diseases. *Gastroenterology* **138**, 1068–1078.

Rose T, Goltstein PM, Portugues R & Griesbeck O (2014). Putting a finishing touch on GECIs. *Front Mol Neurosci* **7**, 88.

Sanders KM, Salter AK, Hennig GW, Koh SD, Perrino BA, Ward SM & Baker SA (2014*a*). Responses to enteric motor neurons in the gastric fundus of mice with reduced intramuscular interstitial cells of Cajal. *J Neurogastroenterol Motil* **20**, 171–184.

Sanders KM, Ward SM & Koh SD (2014*b*). Interstitial cells: regulators of smooth muscle function. *Physiol Rev* **94**, 859–907.

Sergeant GP, Johnston L, McHale NG, Thornbury KD & Hollywood MA (2006). Activation of the cGMP/PKG pathway inhibits electrical activity in rabbit urethral interstitial cells of Cajal by reducing the spatial spread of Ca^{2+} waves. *J Physiol* **574**, 167–181.

Serysheva II HS (1998). Ryanodine binding sites on the sarcoplasmic reticulum Ca^{2+} release channel. In *Structure and Function of Ryanodine Receptors*, ed. Sitsapesan RWA, pp. 95–104. Imperial College Press, London.

Spencer NJ, Bywater RA, Holman ME & Taylor GS (1998). Inhibitory neurotransmission in the circular muscle layer of mouse colon. *J Auton Nerv Syst* **70**, 10–14.

Suzuki H, Ward SM, Bayguinov YR, Edwards FR & Hirst GD (2003). Involvement of intramuscular interstitial cells in nitrergic inhibition in the mouse gastric antrum. *J Physiol* **546**, 751–763.

Tian L, Hires SA, Mao T, Huber D, Chiappe ME, Chalasani SH, Petreanu L, Akerboom J, McKinney SA, Schreiter ER, Bargmann CI, Jayaraman V, Svoboda K & Looger LL (2009). Imaging neural activity in worms, flies and mice with improved GCaMP calcium indicators. *Nat Methods* **6**, 875–881.

van Helden DF, Imtiaz MS, Nurgaliyeva K, von der Weid P & Dosen PJ (2000). Role of calcium stores and membrane voltage in the generation of slow wave action potentials in guinea-pig gastric pylorus. *J Physiol* **524**, 245–265.

Wang XY, Chen JH, Li K, Zhu YF, Wright GW & Huizinga JD (2014). Discrepancies between c-Kit positive and Ano1 positive ICC-SMP in the W/Wv and wild-type mouse colon; relationships with motor patterns and calcium transients. *Neurogastroenterol Motil* **26**, 1298–1310.

Wang XY, Paterson C & Huizinga JD (2003). Cholinergic and nitrergic innervation of ICC-DMP and ICC-IM in the human small intestine. *Neurogastroenterol Motil* **15**, 531–543.

Ward SM (2000). Interstitial cells of Cajal in enteric neurotransmission. *Gut* **47** (Suppl 4), iv40–43; discussion iv52.
Ward SM, Beckett EA, Wang X, Baker F, Khoyi M & Sanders KM (2000). Interstitial cells of Cajal mediate cholinergic neurotransmission from enteric motor neurons. *J Neurosci* **20**, 1393–1403.
Ward SM, Burns AJ, Torihashi S & Sanders KM (1994). Mutation of the proto-oncogene c-kit blocks development of interstitial cells and electrical rhythmicity in murine intestine. *J Physiol* **480**, 91–97.
Ward SM & Sanders KM (2001). Interstitial cells of Cajal: primary targets of enteric motor innervation. *Anat Rec* **262**, 125–135.
Ward SM & Sanders KM (2006). Involvement of intramuscular interstitial cells of Cajal in neuroeffector transmission in the gastrointestinal tract. *J Physiol* **576**, 675–682.
Ward SM, Sanders KM & Hirst GD (2004). Role of interstitial cells of Cajal in neural control of gastrointestinal smooth muscles. *Neurogastroenterol Motil* **16**(Suppl 1), 112–117.
Waterman SA & Costa M (1994). The role of enteric inhibitory motoneurons in peristalsis in the isolated guinea-pig small intestine. *J Physiol* **477**, 459–468.
Wellman GC & Nelson MT (2003). Signaling between SR and plasmalemma in smooth muscle: sparks and the activation of Ca^{2+}-sensitive ion channels. *Cell Calcium* **34**, 211–229.
Wood JD (1972). Excitation of intestinal muscle by atropine, tetrodotoxin, and xylocaine. *Am J Physiol* **222**, 118–125.
Xu W & Lipscombe D (2001). Neuronal Ca(V)1.3alpha(1) L-type channels activate at relatively hyperpolarized membrane potentials and are incompletely inhibited by dihydropyridines. *J Neurosci* **21**, 5944–5951.
Yamamoto M (1977). Electron microscopic studies on the innervation of the smooth muscle and the interstitial cell of Cajal in the small intestine of the mouse and bat. *Arch Histol Jpn* **40**, 171–201.
Zhu MH, Kim TW, Ro S, Yan W, Ward SM, Koh SD & Sanders KM (2009). A $Ca(^{2+})$-activated Cl(-) conductance in interstitial cells of Cajal linked to slow wave currents and pacemaker activity. *J Physiol* **587**, 4905–4918.
Zhu MH, Sung IK, Zheng H, Sung TS, Britton FC, O'Driscoll K, Koh SD & Sanders KM (2011). Muscarinic activation of Ca^{2+}-activated Cl- current in interstitial cells of Cajal. *J Physiol* **589**, 4565–4582.
Zhu MH, Sung TS, O'Driscoll K, Koh SD & Sanders KM (2015). Intracellular Ca^{2+} release from endoplasmic reticulum regulates slow wave currents and pacemaker activity of interstitial cells of Cajal. *Am J Physiol Cell Physiol* **308**, C608–C620.
ZhuGe R, Sims SM, Tuft RA, Fogarty KE & Walsh JV, Jr (1998). Ca^{2+} sparks activate K^+ and Cl- channels, resulting in spontaneous transient currents in guinea-pig tracheal myocytes. *J Physiol* **513**, 711–718.

Additional information

Competing interests

The authors declare that they have no competing interests.

Funding

This project was supported by exploratory research funding from the University of Nevada and from P01 DK41315 from the NIDDK that supported Core laboratories providing molecular and immunohistochemical support. ICC were sorted by the FACS/flow cytometry shared resource laboratory, which is supported by a Phase III COBRE award (P30-GM110767). SB and BD received salary support from R01 DK-091336. KMS and SMW received salary support from P01 DK41315.

Author contributions

SAB, BTD, DS and KMS conceived and designed the experiments. SAB, BTD, GWH, SMW and KMS collected, analysed and interpretated data. SAB, BTD, DS, GWH, SMW and KMS drafted the article and/or revised it critically for intellectual content. All authors have approved the final version of the manuscript and agree to be accountable for all aspects of the work. All persons designated as authors qualify for authorship, and all those who qualify for authorship are listed.

Acknowledgements

We thank Yulia Bayguinov for performing immunohistochemistry; Lauren Peri for the molecular expression studies; Byoung Koh for collecting cells by FACs; and Nancy Horowitz for maintenance and breeding of mice.

Supporting information

The following supporting information is available in the online version of this article.

Movie S1. ICC-DMP spontaneous Ca^{2+} transients. Movie of intracellular Ca^{2+} transients in ICC-DMP labelled with the genetically encoded Ca^{2+} indicator GCaMP3. The top left FOV shows elongated ICC-DMP at 60× and the top right FOV shows ICC-DMP at 100× magnification. Note the lack of coincidence of Ca^{2+} transients between the blue bit-masked cell and the non bit-masked cell in the 100× FOV. The blue ICC-DMP in the FOV was used to construct an ST map of Ca^{2+}-induced fluorescence intensity across the diameter of the cell, which better displays the firing and propagation of Ca^{2+} transients along the length of the cell (lower). Note the stochastic firing of spontaneous Ca^{2+} transients in ICC-DMP.
Movie S2. Long-term recording of spontaneous Ca^{2+} transients in several ICC-DMP within the FOV. Long recording (4 min) Movie of spontaneous ICC-DMP Ca^{2+} transients activity in the murine jejunum. The left window shows the original recordings of ICC-DMP and the right window shows Ca^{2+} transient particles thresholded (SNR $\geq$25 dB) after differentiation ($\Delta t = 0.5$ s) and smoothing (Gaussian 1.0 SD, box size = 3.3 μm).